

Photochemical method for removing methane interference for improved gas analysis

Merve Polat¹, Jesper Baldtzer Liisberg², Morten Krogsbøll¹, Thomas Blunier², and Matthew S. Johnson¹

¹Copenhagen Center for Atmospheric Research, Department of Chemistry, University of Copenhagen, Universitetsparken 5, DK-2100 Copenhagen Ø, Denmark

²Physics of Ice Climate and Earth, Niels Bohr Institute, University of Copenhagen, DK-2100 Copenhagen Ø, Denmark

Correspondence: Matthew S. Johnson (msj@chem.ku.dk)

Abstract. The development of laser spectroscopy has made it possible to measure minute changes in the concentrations of trace gases and their isotopic analogs. These single or even multiply substituted species occur at ratios from percent to sub-ppm and contain important information concerning trace gas sources and transformations. Due to their low abundance minimizing spectral interference from other gases in a mixture is essential. Options including traps and membranes are available to remove many specific impurities. Methods for removing CH₄, however, are extremely limited as methane has low reactivity and adsorbs poorly to most materials. Here we demonstrate a novel method for CH₄ removal via chlorine-initiated oxidation. Our motivation in developing the technique was to overcome methane interference in measurements of N₂O isotopic analogs when using a cavity ring-down spectrometer. We describe the design and validation of a proof-of-concept device and a kinetic model to predict the dependence of the methane removal efficiency on methane concentration [CH₄], chlorine photolysis rate J_{Cl_2} , chlorine concentration [Cl₂], and residence time t_R . The model was validated by comparison to experimental data and then used to predict the possible formation of troublesome side- and by-products including CCl₄ and HCl. The removal of methane could be maintained with a peak removal efficiency > 98 % for ambient levels of methane at a flow rate of 7.5 ml min⁻¹ with [Cl₂] at 50 ppm. These tests show that our method is a viable option for continuous methane scrubbing. Additional measures may be needed to avoid complications due to the introduction of Cl₂ and formation of HCl. Note that the method will also oxidize most other common volatile organic compounds. The system was tested in combination with a cavity ring-down methane spectrometer, and the developed method was shown to be successful at removing methane interference.

1 Introduction

Infrared absorption is a fast, convenient, and non-destructive approach for measuring gas composition used in a wide range of applications. High-resolution instruments based on specific rovibrational transitions are becoming available to characterize the abundance of rare isotopocules within gases. Laser spectroscopy has entered territory that has been the exclusive domain of mass spectrometry. While recent advances in the field can give the impression that new laser-based instruments can be used in a "plug and play" manner, there are still limitations to the accuracy and reproducibility of the measurements.

In a recent study investigating the performance of currently available laser spectroscopic N₂O isotope analyzers (Harris et al. (2020)), a number of interferences from other trace gases were identified, arising from spectral overlap of N₂O and the rovi-

25 brational spectra of the other gases. The consequence was an offset in the measured isotopocule abundance value arising exclusively from ambient levels of methane for a Picarro G5131-i cavity ringdown-based instrument that determines $\delta^{15}\text{N}$, $\delta^{15}\text{N}^\alpha$, $\delta^{15}\text{N}^\beta$, and $\delta^{18}\text{O}$ for N_2O . These instruments are often used to measure isotopic signatures of N_2O emitted from soils, (Ibraim et al. (2019a), Wolf et al. (2015), Yu et al. (2020)), which can help to differentiate distinct microbial and abiotic production pathways.

30 N_2O formation in soils is commonly accompanied by production / uptake of other trace gases such as CH_4 , CO_2 , and water vapor (Erler et al. (2019), Ibraim et al. (2019b)). These variations complicate measurements. An example of the relevant variation of CO_2 and CH_4 can be found in the work of (M. Zimnoch and Rozanski (2010)) where the background level of CH_4 and CO_2 at 1.8 ppm and 380 ppm, can change suddenly to levels above 3.6 ppm and 560 ppm. For the instrument described in Harris et al. (2020), these variations will result in an observed offset in the measured $\delta^{15}\text{N}^\alpha$ of 4.0 ‰ and $\delta^{18}\text{O}$ of 1.1 ‰ (Harris et al. (2020)). The change in CH_4 results in an apparent increase of 4.6 ‰ and 2.2 ‰ for $\delta^{15}\text{N}^\alpha$ and $\delta^{18}\text{O}$ respectively, while the change in CO_2 results in a decrease of 0.6 ‰ and 1.1 ‰ for $\delta^{15}\text{N}^\alpha$ and $\delta^{18}\text{O}$ respectively. As the effect of variation in these two trace gasses lead to opposed offsets in the measured isotopologues, it greatly decreases both the accuracy and precision of the G5131-i. It is therefore essential for accurate measurements to account for these interferences.

One solution is multi-line analysis, or careful measurement of the interfering gas(es) with a second instrument. These options are not desirable for all applications as they either require a redesign of the instrument or investment in additional equipment, and these corrections can introduce additional uncertainty. A more direct and practical method would be to remove the interfering species from the sample. For discrete sampling the best method would be to separate the N_2O from the sample matrix and release it into a well defined matrix for interference-free measurements.

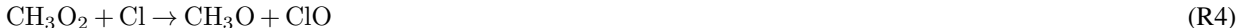
For on-line measurements, well-established methods including chemical traps and membranes are readily available for the removal of CO_2 , CO , and humidity. However, to the best of our knowledge, no method for continuous removal of methane is available with the exception of catalyzed combustion (Cullis and Willatt (1983)) which requires high temperatures and the addition of oxygen thereby altering the gas matrix. It was desired to develop a method for removing CH_4 and potentially other VOCs in a manner that would only introduce minimal changes to the matrix composition.

Inspiration for the method investigated in this work was taken from the oxidation pathways taking place in the atmosphere (Pugliese (2018)). The majority of methane is oxidized through an initial reaction with OH radicals (Rigby et al. (2017)) that results in the formation of H_2O and CH_3 radicals. However, the chlorine radical is a potentially important agent in initiating chain reactions: Generally, the reaction rates of Cl with VOCs exceed the analogous ones with OH by at least one order of magnitude. The rate constant for methane's reaction with Cl radicals is $1.07 \cdot 10^{-13} \text{ cm}^3 \text{ molecules}^{-1} \text{ s}^{-1}$ (Bryukov et al. (2002)) and with hydroxyl radicals is $6.20 \cdot 10^{-15} \text{ cm}^3 \text{ molecules}^{-1} \text{ s}^{-1}$ (Bonard et al. (2002)). The reason for the limited role of chlorine in the global atmosphere is that it's concentration on average is three or four orders of magnitude lower than OH, although it can have an impact in the stratosphere and in marine and polar environments. The mechanism for Cl-initiated

Table 1. Table summarizing experiments and setups. See Figure B1 for overview. FC: Flow controlled. CWL: Chlorine waste line. PC: Pressure controlled.

Setup	Description	Experiments
1	High-Pressure Xenon Lamp with FC CWL	A
2	Single Tube Hexagonal Photochemical Device with FC CWL	B
3	Single Tube Hexagonal Photochemical Device with with PC CWL	C, D, E
4	Multiple Tubes Hexagonal Photochemical Device with PC CWL	F, G, H, I

methane oxidation technology proposed in this study is outlined in reactions: (R1) -(R6).



We demonstrate a novel method for CH_4 removal through chlorine initiated oxidation. Using four experimental setups, we show that methane removal is highly dependent on the flow, chlorine mixing ratio, and light source. We developed a simple kinetic model to predict the removal efficiency as a function of the four key parameters in the system; $[\text{CH}_4]$, J_{Cl_2} , $[\text{Cl}_2]$, and residence time t_R . The model includes essential reactions and additional estimated radical-wall reactions. Two approaches for estimating the photo-dissociation rate of Cl_2 are presented. The goal is to determine the effect of these variables and achieve the desired methane removal efficiencies by optimizing the parameters. The goal is to achieve removals above 99 % for methane at low to ambient concentrations. With the method developed and refined, a final set of experiments is conducted using a Picarro CRDS model G5131-i, capable of measuring N_2O mixing ratio and its isotopic abundance. The measured values of $\delta^{15}\text{N}^\alpha$ and $\delta^{18}\text{O}$, subject to methane interference, are compared to data corrected for methane levels, as these corrected isotopologue levels remained stable across the experiment.

2 Method

2.1 Experimental approach

2.1.1 Methane experiments

Four different variations of the setup seen in Figure 1 are used during our experiments, summarized in Table 1 together with which experiments they were used for.

Table 2. Table summarizing experimental conditions.

Flask name	CH ₄ / ppm	Cl ₂ / ppm	N ₂ O / ppb	Matrix composition	Flow range / (ml min ⁻¹)
I	0	100 ± 2.5	0	>99 % N ₂	6-23
II	2.003 ± 5 · 10 ⁻⁴	0	323	Atmospheric air	1-29
II	78 ± 2	0	0	20.95 % O ₂ + >79 % N ₂	0.3-1.2
IV	0	0	509	0.95 % Ar + 20.95 % O ₂ + >78 %	28-50

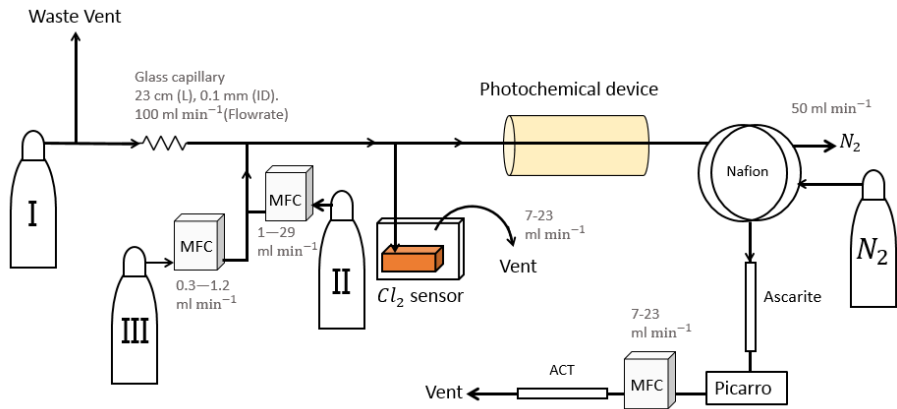


Figure 1. General setup. ACT: Activated Carbon Trap. MFM: Mass Flow Meter. MFC: MKS Mass Flow Controller GE50A. mfc: manual flow controller. Table 2: Gas flask. Four variation of the general setup is performed. The setup variations and the experiments performed with the setup is shown in Table 1. Setup 1 uses a Xenon lamp as the photochemical device. Setups 2-4 uses the same photochemical device, which consists of 420 LEDs. The chamber tube used in Setups 1-3 is one quartz tube (20 cm (L) x 12.7 mm (OD)), while setup 4 uses seven smaller quartz tubes. Five with the size 8.33 mm (OD), 6.33 mm (ID) and 20 cm (L), and two with the size 8.33 mm (OD), 6.33 mm (ID) and 25 cm (L). The setups also differ in the chlorine waste line. Setups 1-2 uses a flow-controlled chlorine waste line, while setups 3.4 uses a pressure-controlled Chlorine Waste line.

The system, Figure 1, has a manifold combining flows from two channels: the sample channel and the chlorine gas channel. [Cl₂] is supplied from an external tank labelled flask I (see Table 2 for gas flask). Atmospheric air, flask II, is combined with an enriched source of [CH₄] in flask III to generate various levels of [CH₄] for the sample channel. A chlorine sensor is placed outside the main flow line to reduce the volume of the setup and allow for increased time-resolution. The flow containing methane and chlorine gas is split at a T-piece, where the main flow proceeds through the photochemical device with excess gas going past a Cl₂ sensor. (Chlorine Gas Detector 0-20 ppm Cl₂). Cl₂ concentrations above 20 ppm are estimated from the flow rate ratios.

The Photochemical device

Setup 1 uses a High-Pressure Xenon Lamp (ILC technology R100-IB) as the photochemical device. Setups 2-4 use a photochemical chamber consisting of 420 LED with peak emission at 365 nm with the circuit board mounted together in a hexagonal cylinder. (illustrated in Figure B2) The 420 LED are connected in parallel. At the maximum voltage of 3.8 V each consumes

90 13.2 mA resulting in a total power of 21 W.

A single quartz with 20 cm in length and 12.7 mm in outer diameter is used as the chamber tube for setups 1-3. In setup 4, the t_R in the chamber is increased by a factor of 2.7 by substituting a single quartz tube with seven smaller quartz tubes in hexagonal shape for optimal packing comprising five tubes OD: 8.33 mm, ID: 6.33 mm and L: 20 cm and two tubes with dimensions OD: 8.00 mm, ID: 6.00 mm and L: 25 cm. The tubes were connected in series via Tygon tubes, Tygon R3603, of
95 length 5 cm. The insides of these tubes were coated with krytox (DuPont GPL 205 Krytox Performance Grease), to prevent reaction with Cl_2 .

Post photolysis scrubbing

After the photochemical device the sample passes through a 35 cm Nafion membrane (TT-030 from Perma Pure LLC). The dried sample then passes through an ascarite trap consisting of a central layer of NaOH between two layers of $\text{Mg}(\text{ClO}_4)_2$
100 separated by glass wool. These types of traps are normally used for the removal of CO_2 and H_2O (Harris et al. (2020)), but they were found to likewise remove HCl and Cl_2 . This removal was confirmed by separate experiments, as it was essential none of the corrosive gasses made it to the delicate Picarro instrument. The gas stream then flows into a cavity ring-down spectrometer (CRDS), the Picarro model G1301. A nominal flow of 15 ml min^{-1} was maintained with the exception of experiments involving variation in t_R when this flow was changed accordingly. At the outlet of the Picarro G1301 an activated
105 carbon (Bead-Shaped Activated Carbon, KUREHA Corporation) trap labeled "ACT" is attached, which is mainly used for scrubbing chlorinated organic species, such as CCl_4 , out of health concern (Ryu and Choi (2004), Milchert et al. (2000)).

2.1.2 N_2O Experiments

A final set of experiments is conducted using a Picarro CRDS model G5131-i, capable of measuring N_2O mixing ratio and isotopic abundance. These experiments were performed to validate the effect of the removal of CH_4 on the measurement of
110 N_2O . These experiments were done in two sets using the setups Figure B1e and Figure B1f. The difference between the two setups was the inclusion of a sofnocat trap in Figure B1f. The sofnocat trap is used to oxidize the CO product (Harris et al. (2020)) and was prepared with 1.25 g of sofnocat contained in a 1/4" SS tube of length 8 cm kept in place by glass wool.

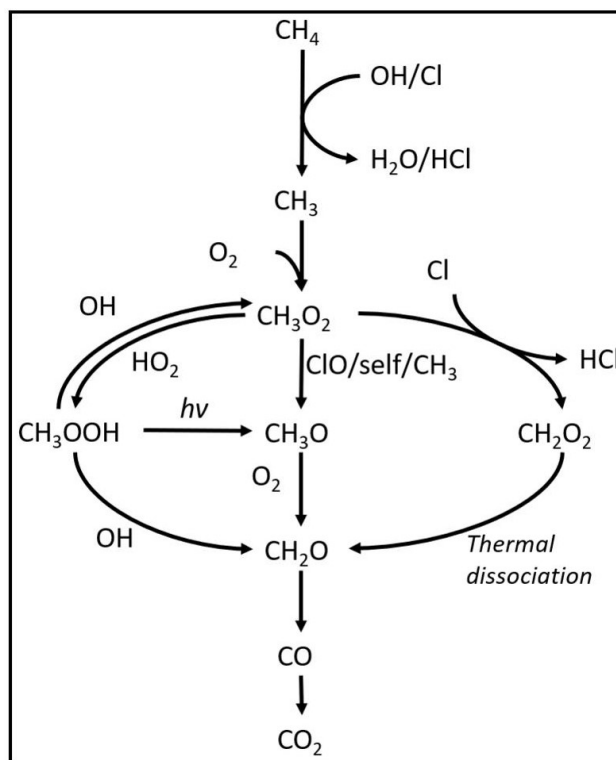


Figure 2. Reaction scheme for the oxidation of methane to CO_2 . CH_3O_2 self reactions lead to the formation of CH_3O .

2.2 Theoretical approach

2.2.1 Kintecus, Version 6.8

115 A model is made with the program Kintecus, version 6.8, (Ianni (2012)) to investigate the reaction mechanisms in the photochemical device. The model contained the relevant reactions with rates for chlorine atom production and removal, methane oxidation, and formation of chlorinated species. The model was kept as simple as possible while still including the relevant reactions. The reactions used in the model are found in Tables E1 - E3. A simplified reaction-scheme is shown in Figure 2. A continuous flow was simulated by setting the initial and external concentrations of gases flowing through the chamber to the

120 same value. This is done for the gases: Cl_2 , CH_4 , N_2 and O_2 . A copy of the model parameters is available in the Appendix C.

Radical wall reactions

A set of radical terminating reactions is incorporated in the model to account for reactions on the walls of the quartz tube.



The wall reactions are assumed to be diffusion limited. The diffusion length is calculated as the average distance from the wall. The diffusion length and rate were calculated using equations (1) and (2), respectively. The estimate of the diffusion rate is described in detail in the section C1. The diffusion constants, diffusion lengths, and estimated wall reaction rates are shown in Table C1.

$$l = r \cdot \left(1 - \frac{1}{\sqrt{2}}\right) \quad (1)$$

Where l in the diffusion length and r being the inner radius of the tube.

$$k = \frac{4 \cdot D}{l^2} \quad (2)$$

135 Where D is the diffusion constant (see table C1).

Model results

The outputs from the model are the photodissociation-rate, J_{Cl_2} , and the abundance of $[\text{Cl}]$ and the production of CCl_4 as an indicator of the production of unwanted side-products.

J_{Cl_2} estimation

140 The chlorine photolysis rate, J_{Cl_2} , is estimated in two ways, which is described in more detail in the section C2. The first approach is to fit J_{Cl_2} to reproduce the observed removal efficiencies from the experimental results. These fits were performed for experiments investigating the effect of power.

A second approach is to estimate J_{Cl_2} by relating it to the electric power going through the circuit, P_{IN} . Based on our observation, a second-order polynomial provided the best fit to describe the effective light output, P_{eff} as a function of P_{IN} .

$$145 \quad P_{\text{eff}}(P_{\text{IN}}) = (a \cdot P_{\text{IN}} + b) \cdot P_{\text{IN}} \quad (3)$$

Where the constants a (W^{-1}) and b (unitless) are experiment-dependent constants that scale the effective light output P_{eff} in W. From the effective power output, the photolysis rate J_{Cl_2} is calculated by eq.(4).

$$J_{\text{Cl}_2}(\text{W}) = P_{\text{eff}}(P_{\text{IN}}) \cdot J_{\text{scale}} \quad (4)$$

150 J_{scale} (J^{-1}) is the scaling-factor and was calculated from the cross-section of Cl_2 , the wavelength distribution of the generated light, and the expected photon density. The density of photons depends on the volume and cross-section of the tube within the photochemical device. J_{Cl_2} is fit to the data collected for some of the experimental steps for exp. D and I. Exp. D reflects the Single Tube system (Setups 1-3) while experiment I reflects the optimized Multiple Tubes system (Setup 4). From the fitted a , b , and calculated J_{scale} the photolysis rate could be calculated for the other experiments.

3 Results and Discussion

Table 3. Removal efficiencies in % for experiments C-I.

Step	C	D	E	F	G	H	I
RE%							
1	45 ± 5	17.6 ± 0.6	22 ± 12	28.0 ± 0.3	47.4 ± 1.2	68 ± 3	46.1 ± 1.8
2	18.9 ± 1.3	24.82 ± 0.5	19.8 ± 1.9	37.3 ± 0.3	54.7 ± 0.5	88.1 ± 1.3	56.6 ± 0.2
3	27.8 ± 1.0	15.4 ± 0.3	16.7 ± 1.2	46.83 ± 0.1	60.8 ± 0.5	92 ± 5	64.29 ± 0.1
4	61 ± 9	6.2 ± 0.3	23.1 ± 1.9	53.77 ± 0.1	66.2 ± 0.6	94 ± 5	70.31 ± 0.1
5		38.2 ± 1.8	35 ± 3	55.2 ± 0.1	69.6 ± 0.3	96 ± 4	75.09 ± 0.1
6		33.6 ± 0.9	29.3 ± 1.6	58.0 ± 0.3	72.0 ± 0.4	98.99 ± 0.1	82.28 ± 0.07
7		37.0 ± 1.3	39 ± 6	59.2 ± 0.3	74.1 ± 0.6	96.7 ± 0.3	83.25 ± 0.04
8		33.1 ± 1.5	40 ± 5		77.2 ± 0.7	87.33 ± 0.1	
9		35 ± 15	35 ± 2		60.3 ± 0.4	77.30 ± 0.1	
10		37 ± 14	45 ± 4		60.2 ± 0.2		
11			47 ± 2		64.0 ± 0.2		
12			41.0 ± 1.9		66.1 ± 0.3		
13			54 ± 2				
14			53 ± 3				
15			45 ± 3				
16			59 ± 2				

155 3.1 Experimental results

The findings are based on twelve experiments, named A-L, containing multiple steps of turning on the photolysis under different conditions. These steps will be referred to by their experimental letter and their number, eg. experiment C step 5 would be exp. C5. An overview of the settings and resulting removal efficiencies for experiments C-I can be seen Table 3 (See Appendix Tables D1 - D3). Table 1 gives an overview of the experiments. As an example of our data, we present the results from
 160 experiment H, Figure 3, during which we achieved our highest level of removal. The experiment was carried out with constant $[CH_4]_{initial}$, and $[Cl_2]$ at 2.000 ± 0.003 ppm and 50.5 ppm. The different levels of removal seen reflect step-wise changes to the settings for t_R and P_{IN} . As seen in Figure 3 for exp. H1-H4, removal efficiency is improved as the P_{IN} is increased. Starting with H5 a fan was installed to limit temperature increases. P_{IN} was kept at the same level while the residence time in

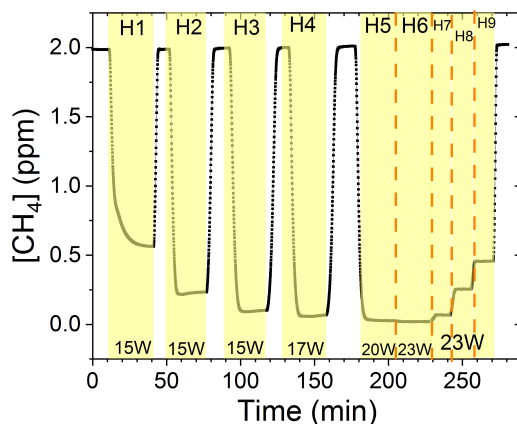


Figure 3. Exp. H. The $[\text{CH}_4]$ is seen as a function of time. The highlight indicates the illumination times. In addition, the experimental step is indicated at the top and P_{IN} (W) is indicated at the bottom

the chamber was decreased. The three steps, (H1-H3), were carried out with constant P_{IN} at 14.8 W with t_R ranging from 164-
 165 350 s. t_R was kept at 350 s for experiments H3-H6. Furthermore, P_{IN} was varied within the range of 14.8-22.8 W. Two issues
 affected the results. First, the system was not initially stable. We believe this is due to a build-up of moisture on the glass-walls,
 coming to equilibrium after the first step, as can be seen from the slope in step H1. Second, there is a small continuous pressure
 drop from the Cl_2 regulator, which leads to a decrease in Cl_2 and an increase in CH_4 . The reason for this was insufficient drying
 of the regulator prior to use, which left a layer of moisture to react with chlorine, thus initiating corrosion in the regulator. This
 170 is also the reason we needed a chlorine waste-line, as a high flow through the regulator was needed to minimize reduce the
 effect of this loss to the regulator. We have accounted for the effect of the pressure drop, but it contributes to the uncertainty of
 our reported Cl_2 . We must press the importance of proper drying prior to the use of Cl_2 gas for people intending to emulate our
 setup.

Effect of Residence Time (t_R (s))

175 Increasing the residence time results in increased removal of methane, shown in Figure 4a. The t_R was investigated in the
 Single and Multiple Tube systems. The same flow rate yields a longer t_R for the multiple tube setup due to the 2.7 fold volume
 increase. The expected trend of asymptotically approaching 100 % can be seen for exp. H, where the high P_{IN} approaches
 more quickly. The effective light output and t_R are lower for experiments B, C and D compared to H. The resulting removal
 of methane is accordingly lower. Increasing the t_R is an easy way of enhancing the removal but at the expense of a slower
 180 response time of the system.

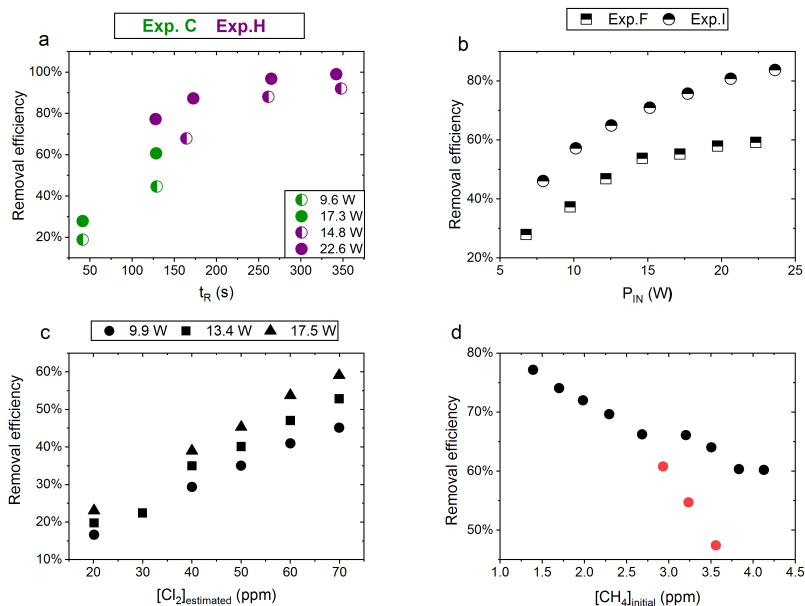


Figure 4. **a.** RE% of methane plotted against t_R (s). The result originates from the three experiments, C (Green) and H (Violet). The experiments have different settings in P_{IN} , $[CH_4]$ and $[Cl_2]$. **b.** RE% of methane plotted against P_{IN} (W). The result are from the three experiments, F (Square) and I (Triangle), which have different $[CH_4]$ settings. **c.** The Figure presents the methane RE% as a function of the chlorine mixing ratio for exp. E. Step one, at 30 ppm $[Cl_2]$, is an example of start-up-deviation, therefore, it is removed. The points represent the three different P_{IN} of the photochemical device. **d.** The Removal efficiency RE% during Exp. G of methane is displayed as a function of the initial methane concentration with the remaining fixed parameters such as $[Cl_2]$ mixing ratio, t_R , and P_{IN} input. The three red points in the Figure represent steps suffering from start-up-deviation.

Effect of Power input (P_{IN} (w))

The results from experiments with power variations are shown in Figure 4b . As presented for exp. F the system reaches a maximum removal efficiency, such that increasing the power does not yield significantly higher removal efficiencies. The $[Cl_2]$ and t_R for experiments F and I is found to be 50 ± 5 and 162 ml min^{-1} , respectively. Comparing exp. F to I it is evident a
185 higher removal efficiency has been reached thanks to the addition of a fan to distribute the heat and prolong the lifetime of the LED's.

Effect of $[Cl_2]$

Exp. E determined the effect of changing $[Cl_2]$, see Figure 4c . $[Cl_2]$ is set between 20 ppm and 70 ppm. Higher $[Cl_2]$ levels result in an increased methane removal rate. The resulting removal efficiency is still below 60 % and the RE% appears to be
190 linear with $[Cl_2]$. Given the result from exp. E the level of $[Cl_2]$ was set to 50 ppm for the remaining experiments.

Effect of initial [CH₄]

Exp. G, plotted in Figure 4d, spans [CH₄] in the range 1.4 - 3.8 ppm. Steps G1-G3 are highlighted to indicate the initial instability. The experiment showed high removal of methane at ambient concentrations.

195 The performance of the experimental setup has been investigated in the aforementioned experiments. The removal efficiencies can be increased by increasing P_{IN} or [Cl₂] resulting in an increase in [Cl]. The negative correlation for [CH₄] is understandable as RE% is a relative value. As expected, the absolute amount of removed methane scales with the [CH₄].

Table 4. Experimental data for the N₂O experiments using the G5131-i for N₂O analysis. Columns: Experimental steps, initial [CH₄] in ppm, residence time in seconds, removal efficiency in %, [N₂O] in ppb, $\delta^{15}\text{N}^\alpha$, $\delta^{15}\text{N}^\beta$ and $\delta^{18}\text{O}$ in ‰ refers to the three isotopologue measurements of N₂O. Each of the three isotope values have been corrected for the effects of oxygen, CO and N₂O variation according to the method described in Harris et al. (2020). The values have not been bound to an absolute scale by the use of calibration gas, so the daily isotopes levels unaffected by methane are shown in the day.

Experiment (#)	CH ₄ <i>initial</i> (ppm)	<i>t_R</i> (s)	R.E. (%)	N ₂ O (ppb)	$\delta^{15}\text{N}^\alpha$ (‰)	$\delta^{15}\text{N}^\beta$ (‰)	$\delta^{18}\text{O}$ (‰)
Exp.J							
1	2.4048 ± 6E-03	64 ± 5	28.3 ± 0.5	340.2 ± 0.03	3.2 ± 1.0	-1.7 ± 0.8	2.6 ± 0.4
2	2.4048 ± 6E-03	64 ± 6	29.5 ± 0.2	338.3 ± 0.04	4.5 ± 0.9	0.8 ± 0.9	3.7 ± 0.5
3	2.4048 ± 6E-03	86 ± 7	34.2 ± 0.2	339.5 ± 0.03	3.6 ± 0.6	0.0 ± 0.8	2.6 ± 0.4
4	2.4048 ± 6E-03	128 ± 10	52.2 ± 0.1	338.2 ± 0.04	1.7 ± 0.6	-1.0 ± 0.8	-0.8 ± 0.4
5	2.4048 ± 6E-03	513 ± 40	84.8 ± 0.1	354.9 ± 0.02	1.0 ± 0.6	0.4 ± 0.7	-0.8 ± 0.5
Exp.K							
1	2.419 ± 1.0E-02	117 ± 9	37.4 ± 2.7	342.5 ± 0.05	4.5 ± 0.5	-1.9 ± 0.7	2.1 ± 0.4
2	2.430 ± 2E-03	117 ± 9	44.2 ± 0.3	337.2 ± 0.03	2.3 ± 0.7	0.1 ± 0.7	2.1 ± 0.5
Exp.L							
1	2.268 ± 1E-03	117 ± 9	43.5 ± 2.0	316.4 ± 0.05	3.7 ± 0.5	-1.7 ± 0.6	1.6 ± 0.4
2	2.406 ± 4.0E-02	89 ± 7	38.0 ± 1.3	329.8 ± 0.09	3.4 ± 1.2	0.5 ± 0.8	2.2 ± 0.8
3	2.406 ± 3E-02	135± 10	54.3 ± 6.8	337.8 ± 0.19	2.6 ± 0.5	0.0 ± 0.5	1.5 ± 0.4
4	2.4018 ± 3E-03	86 ± 7	37.3 ± 0.8	337.7 ± 0.14	3.8 ± 1.4	1.6 ± 0.9	1.7 ± 0.7
5	2.4018 ± 7E-03	141 ± 11	56.8 ± 0.5	338.2 ± 0.13	1.7 ± 0.5	-0.3 ± 0.6	1.1 ± 0.4

3.1.1 N₂O experimental results

200 In Figures 5a and 5b the effects on the isotopic signal of $\delta^{15}\text{N}^\alpha$ and $\delta^{18}\text{O}$ from the removal of methane can be seen. The delta values are self-referenced to the gas without the addition of CH₄. The results are from experiment L, where a softnocat trap had been installed to remove the CO formed by the CH₄ oxidation. By applying the trace-gas and matrix interference

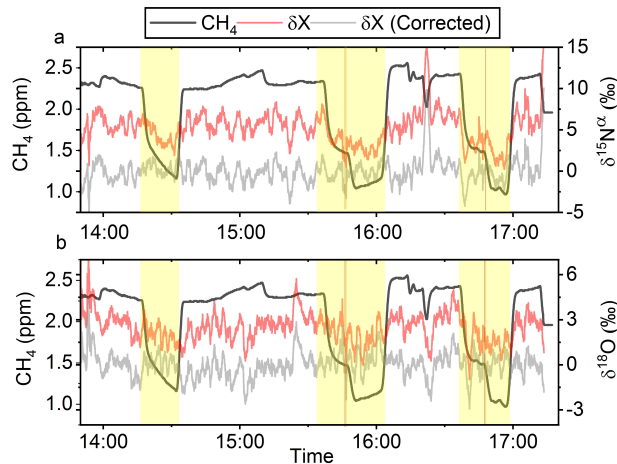


Figure 5. a. Measurements of $\delta^{15}\text{N}^\alpha$ during exp. L in ‰. Red highlights a 100 s averaged measured values corrected for O_2 , CO and CO_2 effects, while grey line indicates a 100 s average values corrected for all interference including CH_4 . The black line shows the CH_4 level in ppm. **b.** Measurements of $\delta^{18}\text{O}$ from exp. L in ‰. Red highlights a 100 s averaged measured values corrected for O_2 , CO and CO_2 effects, while grey line indicates a 100 s average values corrected for all interference including CH_4 . The black line shows the CH_4 level in ppm.

corrections described in Harris et al. (2020) in combination with the measurements of CH_4 , it was found that the isotopologue levels remained stable through the oxidation (grey line). The offset from this corrected value is plotted in (red) showing several ‰ higher values. These levels stabilized during the oxidation in accordance with the drop in methane, thus demonstrating the efficiency of the method. The stability of the corrected isotopic values across the experiment shows that the oxidation does not introduce other components that would interfere with the signal, which are not removed by the traps. Variations of roughly 5 % were observed in $[\text{N}_2\text{O}]$ but are accounted for by variations in the flow of $[\text{Cl}_2]$, thus changing the dilution, rather than formation of N_2O due to the photochemistry. In 4 the results from the three experiments J, K and L can be seen. In the N_2O experiments it was not possible to apply the same conditions that lead to the highest levels of removal presented in the earlier experiments. The reason for this was the addition of the G5131-i increased the minimum flow through the photo-chemical-device, thus decreasing the maximum residence time. Additionally not having a high concentration N_2O source capped the dilution, as the N_2O needed to remain in the linear range of the G5131-i. The limit on the dilution therefore also limited the concentration of Cl_2 available. With a higher concentration Cl_2 source available and a properly prepared regulator, the setup would have been able to deliver sufficient CH_4 removal for more than 24 hours, at which point the ascarite trap would need replenishment.

3.2 Model results

Parameters a and b in eq. (3) were determined from the experimental data. For the single tube system the values were fitted to steps D2 and D6-D9. Here two linear regimes were found, and were fitted by two sets of a and b constants. In this way we

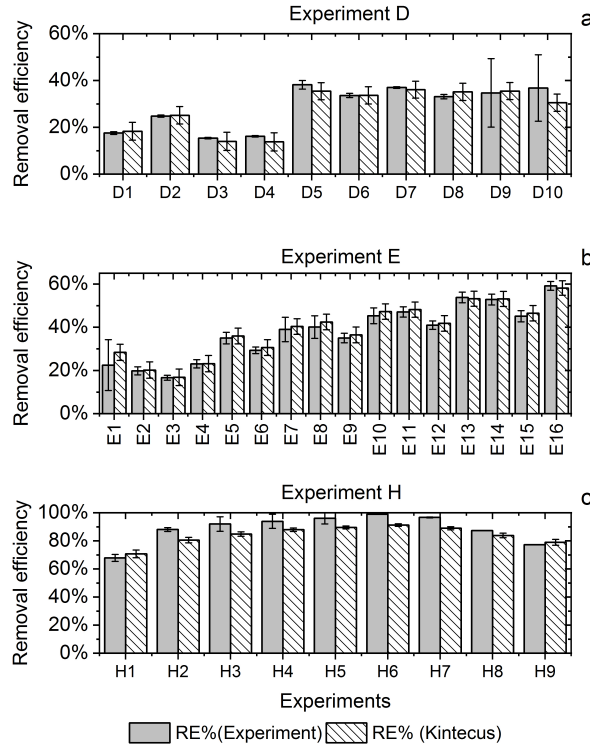


Figure 6. RE% for the steps of exp. D, F and H as found experimentally (White stripes) and by the model (Grey). **a.** Steps D2 and D6-D9 were utilized to generate J_{Cl_2} for the single tube system. **b.** Exp.E **c.** Exp.H

could describe the effect of the thermal management system used in later experiments.

220 The J_{Cl_2} for the single tube systems is obtained from equations (C19) and (C20) (Figures C1c and C1a). These equations are used to calculate J_{Cl_2} for exp. B, C and D. The comparison between the modeled and experimental efficiency is shown in Figure 6.

J_{Cl_2} was determined using the same method. Exp. I is used to obtain model J_{Cl_2} (Figures C1b-C1d and equation (C21).

In Figure 6c a comparison of experimental and model results are shown for exp. H, D and E. The model yields a good agree-
 225 ment with the experimental results. However, the model slightly underestimates RE% for most of the steps, which is also observed for the other experiments. The initial instability can also be seen for steps D1 and D2 depicted in Figure 6a. Problems due to overheating at high P_{IN} are eliminated with the improved photochemical device resulting in a power effectiveness at 15 W of 0.6 % for the single tube to 9 % for the multiple tube system.

Overall, the simple model does a reasonable job of describing the experimental results although it underestimates the removal
 230 efficiency. One issue is that the model does not do a good job of describing the effect of variations of initial methane concen-

Table 5. Parameter ranges

Parameter	Standard value	Range
Cl ₂	50 ppm	20-100 ppm
CH ₄	2.04 ppm	0.5-50 ppm
Residence time	165 s	40-400 s
P_{IN}	14.5 W	9-31 W
O ₂	10 %	
N ₂	90 %	

trations in exp. G shown in Figure E1e.

Additional model runs are used to estimate J_{Cl_2} of experiments E and F, conducted with a modified device, cf. equations (C22) and (C23)-(C24), respectively. It is clear that adjusting J_{Cl_2} results in a model that more accurately fits the experimental results.

235 **3.2.1 Parameters simulated and compared with experimental results**

Exp. I was chosen as the basis for the final simulation: three parameters are fixed and the fourth varies. The methane removal efficiency, chlorine radical abundance, and the resulting abundance of [CCl₄] are determined. The standard values and the ranges investigated can be seen in Table 5. The resulting removal efficiencies as a function of each of the four parameters Power input P_{IN} (W), Residence time t_R (s), [Cl₂] (ppm) and [CH₄] (ppm) are shown in Figure 7. The model results are
240 compared with the experimental results for the parameters P_{IN} (W), t_R (s) and chlorine mixing ratio (ppm), shown in Figures 4b, 4a and 4c, respectively. A good match in the observed response can be seen. The model is too insensitive to methane concentration and fails to recreate the slope observed from the experimental results. The comparison between the model, Figure 7d , and the experimental results, Figure 4d , shows that the model RE% scale is approximately one-tenth of that of the experimental results. This may simply be due to the temperature dependence of the methane reaction rate. Simulations with an
245 increased k_{Cl+CH_4} resulted in better agreement.

The corresponding Cl₂ photo-dissociation rates for the P_{IN} in Figure 7a ranges from $4.04 \cdot 10^{-3}$ to $2.37 \cdot 10^{-2}$ photons s⁻¹ which is a good match with previous J_{Cl_2} values found for a similar system. (Nilsson et al. (2009))

In addition to the RE%, [Cl] and [CCl₄] are also shown in the aforementioned Figures. Chlorinated side-products such as CH₃Cl and CCl₄ were investigated as another potential concern due to climate (Seinfeld and Pandis (2016)). Figure 7a shows
250 that an increase in Cl₂ concentrations increases the [CCl₄] production. The amounts of carbon tetrachloride formed are under a ppt for initial methane concentrations of tens of ppm i.e. yield on the order of less than 10⁻⁷.

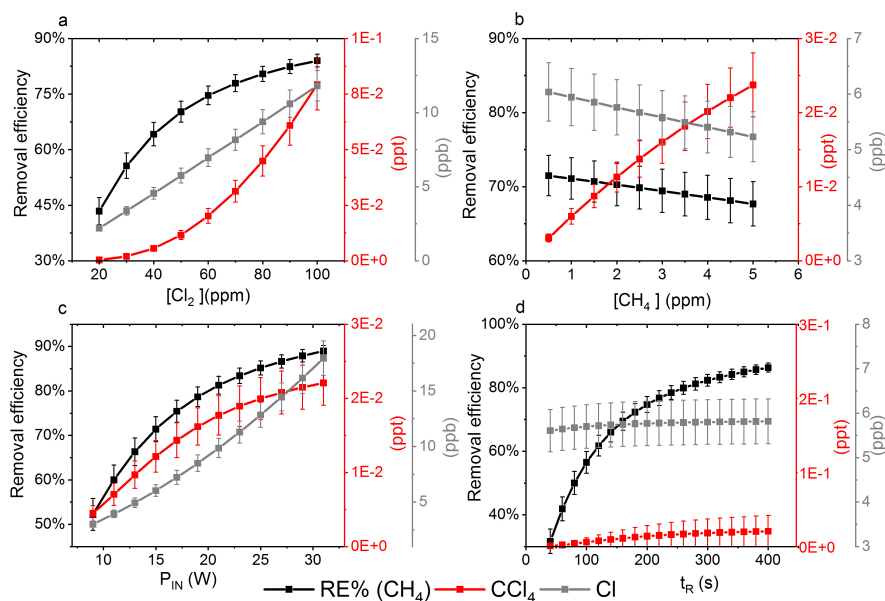


Figure 7. The removal efficiency of methane (Black), [CCl₄] (Red) and [Cl] (Grey) is shown in the Figures a-d. The four parameters are varied while the remaining parameters are kept at the standard parameter presented in Table 5. **a.** The [Cl₂] is varied. **b.** The initial [CH₄] is varied. **c.** The J_{Cl_2} is varied. **d.** The t_R is varied.

3.2.2 Side-reactions and products

The formation of HCl is unavoidable. As expected, the higher photolysis rate leads to more efficient methane-oxidation, and [HCl] rises accordingly. Therefore, scrubber technologies may be necessary, though the use of water bubblers would impose big issues for the reliable measurements of isotopologues. The NO_x concentration in our experiments is insignificant and hence these reactions have not been included in the model.

4 Conclusions

In this study we have described the design, improvement and performance of a process for continuously removing methane from an airstream. The system is based on the photolysis of chlorine gas using UV LED's to generate chlorine atoms. The performance of the setup was investigated on the basis of four variables; [CH₄], [Cl₂], photolysis rate, and t_R .

A model was built and used to describe the chemistry in more detail, and optimize the performance of the process. In addition, the model found that CCl₄ was produced at negligible levels.. The highest removal levels achieved experimentally at ambient methane levels were above 98 % which was maintained under stable conditions. A level above 99.5 % would be achievable by increasing the chlorine concentration or extending the photolysis time. The system was tested using N₂O isotope measurements, a case where methane is known to interfere with measurements of $\delta^{15}N^\alpha$ and $\delta^{18}O$. With the inclusion of a softocat

trap to control CO, the setup was able to remove all interference from H₂O, CO₂, CO and removed 84.5 % of CH₄. While this is not sufficient to remove the effect from CH₄, we are confident that with an optimized setup and settings the method can be used to reliably remove >95 % of CH₄, thereby enabling continuous accurate measurements of [N₂O] and it's isotopically substituted analogues using the Picarro G5131-i.

270 We believe that researchers will be able to use this approach to continuously remove methane from a sample, thereby eliminating interference and improving accuracy.

Appendix A: Proof-of-concept experiments - Preliminary experiments

Proof-of-concept experiments were conducted to investigate the feasibility of the proposed mechanism. The ambient air standard was enriched in Cl₂ by in-situ production of Cl₂, ranging from 1 ppm to <20 ppm, through electrolysis of a saltwater mixture. Following that, the sample was photolyzed in a photochemical device generating Cl radicals. The resulting drop in methane was monitored with a Cavity Ring-Down Spectrometer, Picarro G1301. The photochemical device comprised 28 LEDs (385 nm)(UV LED LAMP-VAOL-5EUV8T4) spaced evenly in a PVS plastic housing. The last set of experiments used a high-pressure Xenon lamp (ILC technology R100-IB) equipped with an optical filter at 335 nm. The resulting peak removal efficiencies for the preliminary experiments are presented in Table A1.

Table A1. Removal Efficiencies for the Preliminary Experiments

Experimental setup (Date)	Highest Stable RE %	Initial [CH ₄] (ppm)
A (17/4)	68 %	2
A (23/4)	67.75 %	1.98
A (24/4)	76.48 %	1.98
B1 (26/4)	78.52 %	2
B2 (30/4)	80.16 %	2
C2 (26/5)	98.20 %.	2

The system yielded an average methane depletion of 86.63 % with a peak depletion at 98.2 %. Various parameters were changed throughout the experiments, and it was determined that the methane depletion is highly dependent on the flow, chlorine production, and light source. A better control of these parameters will yield higher and steadier removal of methane.

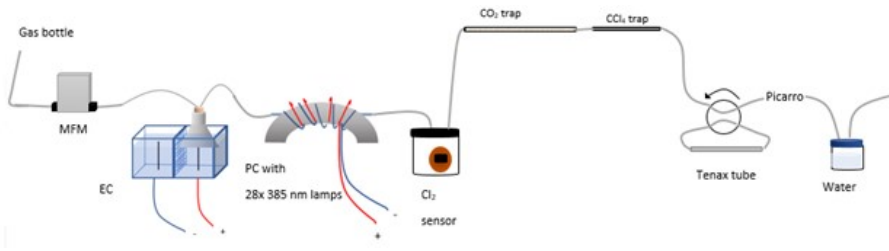


Figure A1. Experimental setup B2 with the inclusion of an activated carbon trap. Gas flask: Ambient air sample, MFM: mass flow meter, EC: electrolytic device, PC: photochemical device.

The experimental setup B2 is presented in Figure A1.

The electrolytic device

285 The experimental setups presented in Table A1 uses an electrolytic device to produce chlorine gas. The electrolytic device is housed in a polycarbonate box. A Nafion membrane, Chemours, Nafion N234, is installed dividing the volume into two half cells. Two electrodes are installed, and the two cells consist of two different solutions of NaCl in milli-Q water. The average concentration of NaCl is 1.3 M at the anodic site and 0.13 M at the cathodic site. The electrodes are carbon electrodes with a diameter of 2 mm and a length of 10 cm. On the anodic side Cl_2 is produced. (Pletcher and Walsh (2012)).

290 Anode reaction:



Cathode reaction:



295

Overall reaction:



The presence of the membrane is essential due to its selectivity to cations. The membrane allows Na^+ ions move from the anode to the cathode and form NaOH. If the membrane was not present the NaOH would encounter Cl_2 and form hypochlorite.

300



305 The electrolysis chamber

In the experimental setups A to B2, Table A1, an electrolysis chamber is used to generate Cl_2 , see Figure A1. The chamber is made from PVC plastic. 28 LED (385 nm), UV LED LAMP-VAOL-5EUV8T4, diodes was installed in the chamber, directed at a quartz tube, OD: 4mm L: 20cm, placed through the chamber. The LED are connected in parallel with a forward voltage and forward current. The max current is 20 mA for each LED, and the max voltage is 3.6 V. The same voltage runs through the LED and the current is multiplied by the number of lamps resulting in 0.480 A.

310

The chlorine gas is introduced into the gas stream by using a funnel above the anode. The water level is adjusted to yield optimal condition for Cl_2 to get into the gas stream and avoid chlorine being deposited on the water surface or water getting sucked into the gas stream.

Additional equipment

- 315 The Picarro G1301 has a cavity pressure at 18.7 kPa, DAS temperature of 30.2 °C and cavity temperature of 45 °C. The gas flask used has an ambient air combined with more stable concentrations of the investigated gases CH₄ (1.98 ppm), CO₂ (376.1 ppm) and H₂O (1.175 % v). The Cl₂ sensor used in all experiments is the PG610-CL2 model, Chlorine Cl₂ Gas Detector Gas Sound Light Vibration Alarm. The sensor measures chlorine concentrations from 1-20 ppm. The sensor is placed in a 600 ml glass flask.
- 320 The general procedure is as follows:
- Prepare solutions
 - Let the system stabilize
 - Turn on the electrochemical device
 - Let the Cl₂ concentration stabilize
- 325
- Turn on lamps
 - Let the system stabilize to ensure a stable RE%.
 - 10 min measurement with Tenax tube sampling (experiments B1 and B2)
 - Turn off the light
 - Let the system stabilize to the initial methane concentration

330 Variations in the experimental setups

Experimental setup A is the initial setup. Experimental setup B1 employed Tenax tube sampling for TD-GCMS measurements of chlorinated species.

Experimental setup B2 follows the same procedure as B1, but with the addition of an activated carbon trap.

- 335 Experimental setup C1 uses a high-pressure Xenon lamp, ILC technology R100-IB. The Xenon lamp lights up the second Photolyze Chamber (PC-2), which is equipped with an 8 mm in diameter and 20 cm in length quartz tube. The inner surface of the cylinder is covered with aluminum foil to reflect the light coming in. The Xenon lamp emits light in wavelengths from vacuum UV (200 nm) to infrared (Moore et al. (2009), therefore a 335 nm optical filter is installed.

At the Picarro G1301 outlet the two traps are used for trapping the gases hydrochloric acid, chlorine gas, and carbon dioxide.

- 340 Experimental setup C2 is similar to C1, however, the Cl₂ concentration is diluted to obtain the values above the fixed value of 20 ppm. At the electrochemical device outlet a union tee divides the flow into two channels, one to the PC-2 and the other to the sensor chamber. The flow at the outlet of the sensor chamber is measured by ADM Flow Meter to ensure a flow of approximately 40-50 ml min⁻¹.

Appendix B: Experimental setups (CH₄ and N₂O)

Table B1. Table summarizing gas flask used in the experiments

Flask name	CH ₄ (ppm)	Cl ₂ (ppm)	N ₂ O (ppb)	Matrix composition	Flow range (ml min ⁻¹)
I	0	100 ± 2.5	0	>99 % N ₂	6-23
II	2.003 ± 5 · 10 ⁻⁴	0	0	Atmospheric air	1-29
III	78 ± 2	0	0	20.95 % O ₂ + >79 % N ₂	0.3-1.2
IV	0	0	500	Atmospheric air	28-50

The photochamber for High Pressure Xenon Lamp (HPXL)-setup uses a quartz tube with dimensions (20 cm in length, 1/2 inches(12.7 mm) in outer diameter) placed in a cylinder coated with aluminium.

The Photochemical Device (PD), Figure B2, for later experiments, Figure B1b - B1f, consists of 420 LED at 365 nm peak wavelength. The LEDs run in a parallel circuit with a forward voltage and forward current (from positive to negative). The max current is 13.2 mA for each LED, and the max voltage is 3.8 V. The same voltage runs through the LEDs, resulting in a total current across the system of 5.5 A.

The difference between the two similar setups STH-PD and STH-PD-MFC are illustrated in Figures B1b and B1c, respectively. Here the forward pressure valve is exchanged with a mass flow controller to allow for a smaller and more stable level of vent flow. The quartz tube of the previous experiments is substituted with seven smaller quartz tubes for MTH-PD setup to yield a longer t_R .

B1 Experimental procedure

- Tune the desired flow from flask C for methane and mix it with a flow from flask B equal to the desired flow plus the intended flow from flask A.
- Let the system stabilize.
- Add the desired flow of chlorine from flask A, by adjusting the pressure at the flask.
- Reduce the flow from flask B by an equal amount to get the desired mixing ratio.
- Let the system stabilize and confirm that the resulting total flow fits with the expected. Make sure the chlorine value can be read on the chlorine sensor.
- When a stable methane level has been run for sufficient time, turn on the photochemical device.

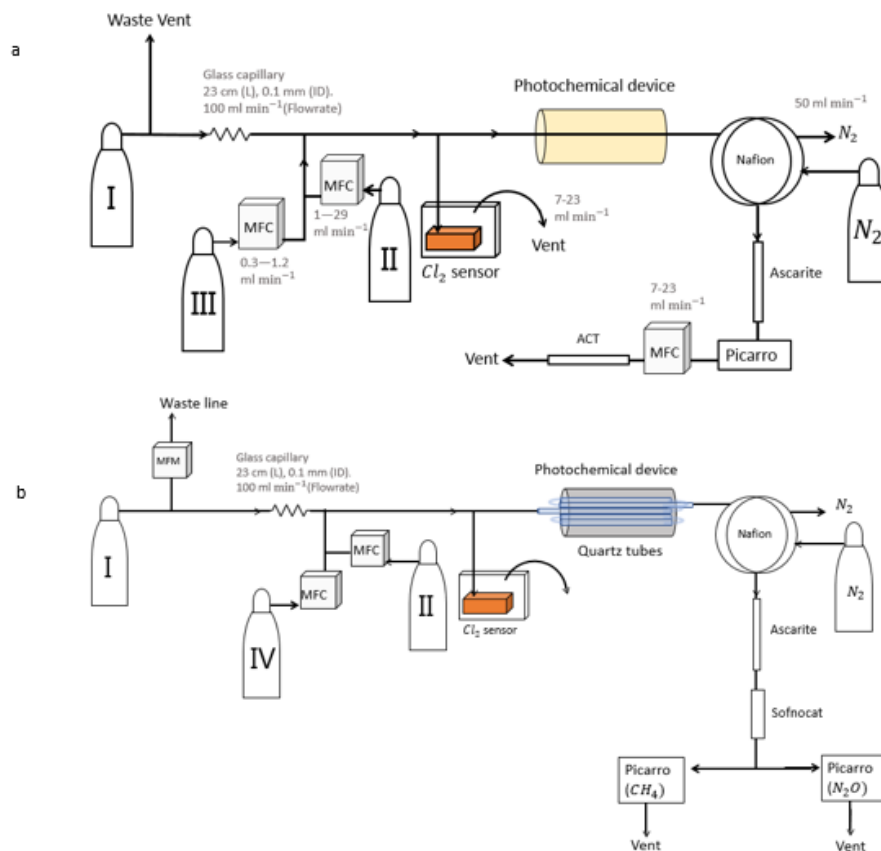


Figure B1. Overview of experimental setups. See Table B1 for gas flask supply. ACT: Activated Carbon Trap. MFM: Mass Flow Meter. MFC: Mass Flow Controller. **a.** Generalized setup for setup 1–4 as was utilized for exp. A–I. Picarro used was G1301. **b.** Setup 6 as used for exp. L. The setup differentiates from setup 5 used for exp. J and K, with the addition of a sofno-cat trap installed immediately following the ascarite trap. Picarro (CH₄): G1301, Picarro (N₂O): G5131-i.

- Let the system stabilize to ensure a stable methane RE%.
- Turn off the light.
- Let the system stabilize to the initial methane concentration before the light was turned on.

B2 N₂O experiments

Experiments were conducted with the Picarro model G5131-i, which is used to measure N₂O mixing ratio and isotopic abundance. The purpose of the experiments was to confirm that the illumination did not affect N₂O. The experimental setups are shown in Figures B1e and B1f. The difference between the two was the inclusion of a sofno-cat trap for oxidizing the formed CO (Harris et al. (2020)). The sofno-cat trap was prepared with 1.25 g of sofno-cat contained in a 6.4 mm diameter tube of

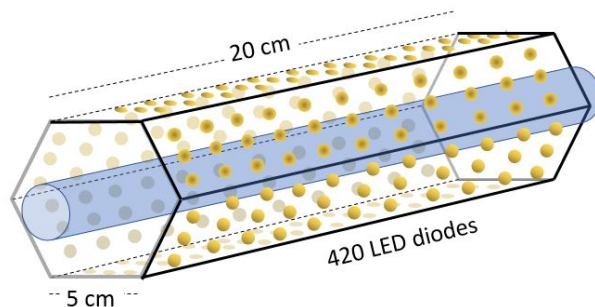


Figure B2. Hexagonal photochemical device consisting of connected circuit boards of 420 LED at 365 nm

length 8 cm and kept in place by glass wool. The trap was installed to prevent effects on the N_2O isotope signal from CO , as presented in (Harris et al. (2020)) the presence of CO 1 ppm gives rise to an erroneous offset in the observed isotopologue values of 1.2, 2.4 and 0.4 ‰ for $\delta^{15}\text{N}^\alpha$, $\delta^{15}\text{N}^\beta$, and $\delta^{18}\text{O}$ respectively. The installation of this trap after the CO_2 trap allowed us to measure the amount of CO present. The technical air from flask C was exchanged with a technical air mix with a 509 ppb [N_2O], allowing for dilution to ambient level. The flow ratio between the three different gases was regulated to maintain a mixing ratio of 330 ppb N_2O , 2.4 ppm CH_4 and 33 ppm Cl_2 . Power supply to the lamp was constant at 4.8 V and 5.0 A, and t_R in the chamber was varied between 86, 117 and 145 s.

Appendix C: Theoretical models

380 The model is made with the program Kintecus, version 6.8, (Ianni (2012)). The model was developed by describing the relevant reactions with rates for chlorine radical production/removal and formation of chlorinated species. The model was kept as simple as possible while still including key reactions. The reactions and their rates used in the model are found in Tables E1 - E3. A simplified reaction-scheme is shown in Figure 2. The experiments are modeled by choosing the concentrations of both the initial and external concentration of used species and the t_R within the chamber. A continuous flow was modeled by setting
 385 the initial and external concentrations of gases flowing through the chamber to the same value. This is done for the gases Cl_2 , CH_4 , N_2 and O_2 .

The physical parameters are fixed as well. The temperature at 298 K, starting integration time to 10^{-6} s (starting step for the integrated model), maximum integration time to 1 s, simulation length equal to t_R plus 5 s, the accuracy of digits to 10^{-4} . Furthermore, the energy unit kcal was selected, and the unit of concentration selected to be molecule cm^{-3} .

390 C1 Radical wall reactions

As described in the main article a set of radical terminating reactions was incorporated into the mode. The wall reaction rates were estimated based on the diffusion rate of the radicals and the diffusion length. The diffusion length is calculated as the average distance from the wall. Because two different sizes of tubes were used throughout the experiments the wall reactions reflects that. The diffusion length and the diffusion rate is given in eq. (C1) and eq. (C2), respectively.

$$395 \quad l = 2 \cdot (D \cdot t)^{0.5} \quad (\text{C1})$$

Where D is the diffusion constant and t is time.

$$k = \frac{1}{t} = \frac{4 \cdot D}{l^2} \quad (\text{C2})$$

The distance, l , is defined as the average distance from the wall, which can alternatively be written as $l = r - d_c$. Where r is the radius of the tube, and d_c is distance from a random particle in the cylinder to the center of the circle of the cylinder. Finding
 400 the average distance to the wall of an infinite number of randomly located particles in the cylinder can be accomplished by solving the equation (C3). The result of eq. (C4) is used to calculate the resulting diffusion rate with the inclusion of the average distance from the walls of the tube, which is defined in eq. (C5).

$$\frac{1}{2}A = \int_0^{d_c} 2r \cdot \pi dr \quad (\text{C3})$$

Where r is the radius and $A = r^2 \cdot \pi$ is the area.

$$405 \quad d_c = \left(\frac{A}{2\pi}\right)^{\frac{1}{2}} = \frac{r}{\sqrt{2}} \quad (\text{C4})$$

$$k = \frac{4 \cdot D}{r - \frac{r}{\sqrt{2}}} \quad (\text{C5})$$

The diffusion constants, diffusion lengths, and estimated wall reaction rates are shown in Table E3.

Table C1. Radical Wall reaction parameters. *Diffusion coefficient is estimated from D_{HO-Air} and D_{HO_2-He} , ** The Chapman and Cowling diffusion model was used to estimate the diffusion constant.

Setup	Reaction	Diffusion constant (cm^2s^{-1})	Reference	Diffusion length (cm)	Wall-reaction rate (s^{-1})
Single tube	$\text{Cl} \rightarrow \frac{1}{2}\text{Cl}_2$	0.260	Judeikis and Wun (1978)	0.146	1.2E+02
Multiple tube				0.091	4.8E+01
Single tube	$\text{ClO} \rightarrow \frac{1}{2}\text{Cl}_2 + \frac{1}{2}\text{O}_2$	0.184	Seinfeld and Pandis (2016)**	0.146	8.8E+01
Multiple tube				0.091	3.4E+01
Single tube	$\text{OH} \rightarrow \frac{1}{2}\text{H}_2\text{O} + \frac{1}{4}\text{O}_2$	0.217	Ivanov et al. (2007)	0.146	1.0E+02
Multiple tube				0.091	4.0E+01
Single tube	$\text{HO}_2 \rightarrow \frac{1}{2}\text{H}_2\text{O} + \frac{3}{4}\text{O}_2$	0.139	Ivanov et al. (2007)*	0.146	6.7E+01
Multiple tube				0.091	2.6E+01

C2 J_{Cl_2} estimation

410 C2.1 First approach

The first approach is to fit J_{Cl_2} in the model to regenerate the observed removal efficiencies from experimental results. These fits were only produced for experiments investigating the effect of P_{in} . The resulting J_{Cl_2} was related to P_{in} via the effective power to light conversion based on the absorption cross-section of Cl_2 and the wavelength distribution of the LEDs. J_{Cl_2} was determined in this manner, once for the single tube systems and once for the multiple tube systems. The photolysis rate J in

415 the units of photons s^{-1} can be determined by equation C6.

$$J_{\text{Cl}_2} = \int \sigma(\lambda, T) \cdot \phi(\lambda, T) \cdot I(\lambda, W) d\lambda \quad (\text{C6})$$

Where $\sigma(\lambda, T)$ is the wavelength dependent cross section of Cl_2 with the unit $\text{cm}^2 \text{ molecule}^{-1}$, $\phi(\lambda, T)$ is the quantum yield, and $I(\lambda, W)$ is the spectral actinic flux density in photons $\text{cm}^{-2} \text{ s}^{-1} \text{ nm}^{-1}$. The cross-section of chlorine dissociation in the range 250-550 nm is defined by C7. (Burkholder et al. (2020))

$$\begin{aligned} \sigma(\lambda, T) = 10^{-20} & \left(\tanh\left(\frac{402.7}{T}\right) \right)^{0.5} \cdot \\ & \left(27.3 \cdot e^{-99.0 \cdot \left(\tanh\left(\frac{402.7}{T}\right) \right) \cdot \left(\ln\left(\frac{329.5}{\lambda}\right) \right)^2} \right. \\ & \left. + 0.932 \cdot e^{-91.5 \cdot \tanh\left(\frac{402.7}{T}\right) \cdot \left(\ln\left(\frac{406.5}{\lambda}\right) \right)^2} \right) \end{aligned} \quad (\text{C7})$$

Where T is the temperature, and λ is the wavelength in nm.

$$I(\lambda, W) = \frac{P(\lambda, W) \cdot D(\lambda) \cdot l}{V} \quad (\text{C8})$$

The actinic flux, eq. (C8) is a function dependent on the power output $P(\lambda, W)$ from eq. (C9), the distribution $D(\lambda)$ from eq. (C11) and the tube volume (V).

$$425 \quad P(\lambda, W) = Eff(W) \cdot \frac{\lambda}{hc} \quad (C9)$$

Where h is planks constant, and c is the speed of light.

It was observed that the photolysis rate did not scale linearly with the applied power, which we speculate may be due to variation of the efficiency of the lamp with applied current and operating temperature. This effect was sufficiently accounted
430 for by a linear fit and is defined as $Eff(W)$.

$$Eff(W) = a \cdot W + b \quad (C10)$$

Where W is the power supplied to the diodes, and values for the constants a and b are fitted in the model to match the experiment. The function C10 accounts for additional variations such as effects due to temperature, the cross-section area of the quartz tube, the conductance of the photochamber and the quality of the distribution fit. This is reflected in the constants
435 a and b varying in response to changes in these parameters. As this is used as a simple empirical stand-in function we do not intend to speculate further on how these changes change the constants.

The photon output, eq. (C9), from the LED was assumed to follow a normal distribution. For this distribution shown in equation (C11), we assumed a center value of 365 nm and FWHM of 10 nm. The distribution, eq. (C11), has units of nm^{-1} .

$$D(\lambda) = \frac{1}{(10\text{nm} \cdot (2\pi)^{0.5} \cdot e^{-0.5 \cdot (\frac{\lambda - 365\text{nm}}{10\text{nm}})^2})} \quad (C11)$$

440 The photolysis rate could then be calculated by eq. (C6) across 250-500 nm at 298 K.

C2.2 Second approach

A second approach for estimating J_{Cl_2} and relating it to P_{IN} was used. This method estimated J_{Cl_2} using simplified kinetics and relating it to power via the same method as the model derived J_{Cl_2} . Exp. F reflects the single tube system while exp. I reflects the optimized multiple tubes setup. Four main reactions, R15 - R18, are considered in the simple kinetic model



$$[k_{Cl+CH_4} = 1.07 \cdot 10^{-13} \cdot \text{molecules}^{-1} \text{cm}^3 \text{s}^{-1}]$$



$$[k_{self} = 1.24 \cdot 10^{-32} \cdot \text{molecules}^{-2} \text{cm}^6 \text{s}^{-1} \cdot [M]]$$



$$[k_{wall} = 124.5\text{s}^{-1} \text{ or } 48.9\text{s}^{-1}]$$

The Cl radicals are consumed at a fast rate, therefore, steady state approximation for Cl has been assumed.

$$\begin{aligned} \frac{d[Cl]}{dt} &= 2 \cdot J_{Cl_2}[Cl_2] - (2 \cdot k_{self} \cdot [Cl]^2 \\ &+ k_{Cl+CH_4} \cdot [CH_4] \cdot [Cl] + k_{wall} \cdot [Cl]) = 0 \end{aligned} \quad (C12)$$

The photolysis rate for the kinetic calculation is, thereby, defined in equation C13

$$455 \quad J_{kin} = \frac{2 \cdot k_{self} \cdot [Cl]^2 + k_{Cl+CH_4}[CH_4][Cl] + k_{wall}[Cl]}{2 \cdot [Cl_2]} \quad (C13)$$

The photolysis rate is calculated from an estimated [Cl] concentration. This was achieved by assuming that the methane concentration would follow an exponential decay with time, equation (C14). The estimated [Cl] is expressed in equation (C15).

$$[CH_4]_t = [CH_4]_0 \cdot \exp(-k_{Cl+CH_4} \cdot [Cl] \cdot t) \quad (C14)$$

460 Where $[CH_4]_t$ is the methane concentration at time t , while $[CH_4]_0$ is the initial concentration.

$$[Cl] = \ln\left(\frac{1}{1 - RE}\right) / (k_{Cl+CH_4} \cdot t) \quad (C15)$$

The values for J_{kin} are generated by inserting the experimental values of $[Cl_2]$, $[CH_4]$ and the estimated value of $[Cl]$ into eq.(C13).

465 The distribution function $D(\lambda)$ from equation (C11) can be used in combination with the cross-section to determine the scale factor J_{scale} .

$$J_{scale}(\lambda, T) = \int_{250\text{nm}}^{500\text{nm}} \frac{\lambda}{hc} \cdot \sigma(\lambda, T) \cdot \frac{l \cdot D(\lambda)}{V} d\lambda \quad (C16)$$

The value of J_{scale} is calculated from the overlap integral between $\sigma(\lambda, T)$ and the emitted photon distribution.

l is the pathlength across the tube/tubes in cm, and V is the volume of the tube/tubes in ml. λ is the wavelength in nm, h is Planck's constant and c is the speed of light. Values for the constants a and b from eq. (C17) are then fitted to match the
470 photolysis rate in eq. (C18) with the photolysis rate found from the Kintecus model.

$$\begin{aligned} P_{eff}(P_{IN}) &= (a \cdot P_{IN} + b) \cdot P_{IN} \\ &= Eff(kin) \cdot P_{IN} = \frac{J_{Kin}}{J_{Scale} \cdot P_{IN}} \end{aligned} \quad (C17)$$

Where P_{eff} is the effective power, and the constants a and b are setup-dependent constants.

From the effective power output the photolysis rate J_{Cl_2} could be calculated by multiplying P_{eff} with J_{scale} .

$$J_{Cl_2}(P_{IN}) = P_{eff}(P_{IN}) \cdot J_{scale} \quad (C18)$$

The J_{Cl_2} is fit to the data collected for some of the experimental steps for exp. F and I to determine the values for the constants a and b .

Exp. F is the single tube system and exp. I is the optimized multiple tube system. From the fitted a , b and calculated J_{scale} the photolysis rate could be calculated for the other experiments.

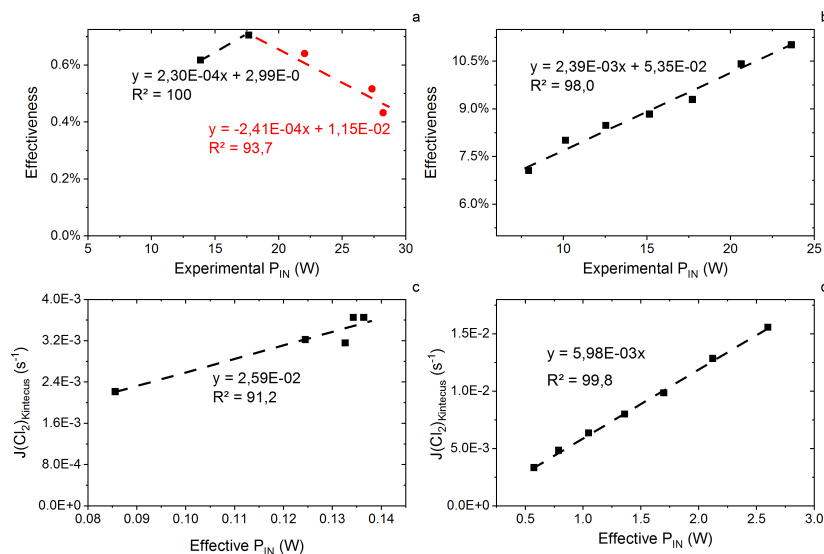


Figure C1. **a.** Effectiveness as a function of experimental power input for exp. D. The correlation is used for calculating the effective P_{IN} for single tube experiments. **b.** Effectiveness as a function of experimental P_{IN} for exp. I. The correlation is used for calculating the effective power for multiple tubes experiments. **c.** Kintecus obtained J_{Cl_2} as a function of the effective p_{IN} for exp. D. The effective p_{IN} is calculated from Figure C1a. The combination of the Figure with Figure C1a is used to calculate the J_{Cl_2} for single tube experiments by Eq. (C19) and (C20). **d.** Kintecus obtained J_{Cl_2} as a function of the effective p_{IN} exp. I. The effective p_{IN} is calculated from Figure C1b. The combination of the Figure with Figure C1b is used to calculate the J_{Cl_2} for Multiple tubes experiments by Eq. (C21)

480 Single tube systems

J_{Cl_2} values are generated on the basis of exp. D2 and D6-D9. The efficiency of p_{IN} is generated from the J_{Cl_2} model. A correlation between effectiveness (%) and experimental p_{IN} (W) is shown in Figure C1a as well as the correlation with the J_{Cl_2} (Kintecus) values in Figure C1c.

The J_{Cl_2} dependence on the p_{IN} (W) for the single tube system, exp. B, C and D, is given by the equations C19 and C20. The
485 equations incorporate a decrease in efficiency of p_{IN} at higher levels due to overheating of the chamber as seen in Figure D2c.

$$J = 2.59 \cdot 10^{-2} \cdot (2.3 \cdot 10^{-4} \cdot (P_{IN})^2 + 2.99 \cdot 10^{-3} \cdot P_{IN})$$

$$if(P_{IN} > 14.67W) \quad (C19)$$

$$J = (2.59E \cdot 10^{-2} \cdot (-2.41 \cdot 10^{-4} \cdot (P_{IN})^2 + 1.15 \cdot 10^{-2} \cdot P_{IN})$$

$$if(P_{IN} < 14.67W) \quad (C20)$$

The comparison between modeled and experimental efficiency for single tube experiment is seen in Figures E1a and E1b.

490 **Multiple tubes systems**

J_{Cl_2} is generated in the same manner as the experiment of results with multiple tubes. Here exp. I is used to obtain model
 J_{Cl_2} -values. (Figures C1b and C1d).

$$J = 5.98 \cdot 10^{-3} \cdot (2.39 \cdot 10^{-3} \cdot (P_{IN})^2 + 5.35E \cdot 10^{-2} \cdot P_{IN}) \quad (C21)$$

The overheating at high p_{IN} is eliminated with the improved photochemical device. This is also apparent when comparing
495 the effectiveness, which is approximately 9 % for the multiple tube configuration, Figure C1b, and approximately 0.6 % for
the single tube system, Figure C1a, at the same p_{IN} at 15 W. Figure E1e and E1f shows the comparison for exp. G and H,
respectively.

Exp. E and F

Some experiments can't be related to the relations presented for the single and multiple tube systems. This is due to the
500 optimization done on the photochemical device. A second approach with additional kinetic calculations is, therefore, used to
estimate the J_{Cl_2} of these two experiments. The effectiveness of exp. E is shown in equation (C22).

$$P_{eff}(P_{IN}) = P_{IN}(-4.35 \cdot 10^{-3} \cdot P_{IN} + 3.26 \cdot 10^{-2}) \quad (C22)$$

In the same manner the effectiveness of exp. F is shown in equations C23 and C24.

$$P_{eff}(P_{IN}) = P_{IN} \cdot (6.80 \cdot 10^{-4} \cdot P_{IN} + 4.36 \cdot 10^{-2})$$

$$if P_{IN} > 14.31W \quad (C23)$$

505

$$P_{eff}(P_{IN}) = P_{IN} \cdot (-1.57 \cdot 10^{-3} \cdot P_{IN} + 7.58 \cdot 10^{-2})$$

$$if P_{IN} < 14.31W \quad (C24)$$

Appendix D: Settings and experimental results

Table D1. Data for exp. A-D. Columns: Experimental steps, [CH₄] (ppm), [Cl₂] (ppm), Residence time t_R (s), Power input p_{IN} (W) and the Resulting removal efficiency in %.

* : The p_{IN} of the xenon lamp was not varied nor determined.

Experiment (#)	CH ₄ (ppm)	Cl ₂ (ppm)	Residence time (s)	Power (W)	Removal efficiency (%)
Exp.A					
1	3.2729 ± 7E-04	16.7 ± 1.	62.4 ± 1.6	*	0.0 ± 0.04
2	2.8327 ± 1.5E-03	25 ± 2	62.2 ± 1.6	*	6.4 ± 0.4
3	2.3769 ± 9E-04	50 ± 5	61.8 ± 1.6	*	27.3 ± 0.4
4	2.9367 ± 3E-03	92 ± 11	62.1 ± 1.6	*	2.7 ± 0.4
Exp.B					
1	3.6391 ± 5E-03	16.7 ± 1.5	60.7 ± 1.6	17.43 ± 0.03	2.0 ± 0.5
2	3.6598 ± 1E-03	16.7 ± 1.5	60.9 ± 1.5	26.13 ± 0.04	6.5 ± 0.2
3	3.7069 ± 1.2E-03	16.7 ± 1.5	62.2 ± 1.6	9.91 ± 0.03	6.9 ± 0.2
4	3.7268 ± 6E-03	16.7 ± 1.5	62.4 ± 1.6	22.09 ± 0.04	11.0 ± 0.6
5	3.919 ± 1.5E-02	50 ± 5	61.0 ± 1.5	9.92 ± 0.03	23.9 ± 0.8
6	3.945 ± 1.4E-02	50 ± 5	61.4 ± 1.5	16.59 ± 0.03	32.7 ± 0.6
Exp.C					
1	3.955 ± 2E-02	50 ± 5	129 ± 4	9.63 ± 0.03	45 ± 5
2	3.957 ± 6E-02	50 ± 5	41.4 ± 1.0	9.63 ± 0.03	18.9 ± 1.3
3	4.0301 ± 5E-03	50 ± 5	41.4 ± 1.0	17.30 ± 0.03	27.8 ± 1.0
4	3.986 ± 1.0E-02	50 ± 5	128 ± 4.7	17.30 ± 0.03	60 ± 9
Exp.D					
1	3.5395 ± 5E-03	32 ± 3	62.5 ± 1.5	13.38 ± 0.03	17.6 ± 0.6
2	3.531 ± 1.5E-02	32 ± 3	85 ± 14	13.85 ± 0.03	24.8 ± 0.5
3	3.5570 ± 8E-03	32 ± 3	43.4 ± 1.1	13.73 ± 0.03	15.4 ± 0.3
4	3.5405 ± 9E-03	32 ± 3	43.0 ± 1.0	13.65 ± 0.03	6.2 ± 0.3
5	3.526 ± 4E-02	32 ± 3	135 ± 58	13.63 ± 0.03	38.2 ± 1.8
6	3.5261 ± 3E-03	32 ± 3	84 ± 2.6	17.65 ± 0.03	33.6 ± 0.9
7	3.564 ± 5E-02	32 ± 3	83 ± 2.2	22.05 ± 0.04	37.0 ± 1.3
8	3.567 ± 5E-02	32 ± 3	83 ± 2.2	28.22 ± 0.04	33.1 ± 1.5
9	3.5729 ± 3E-03	32 ± 3	83 ± 2.2	27.34 ± 0.04	35 ± 15
10	3.5447 ± 7E-03	32 ± 3	79 ± 2.1	33.10 ± 0.04	37 ± 14

Table D2. Data for exp. E-F. Columns: Experimental steps, [CH₄] (ppm), [Cl₂] (ppm), Residence time t_R (s), Power input p_{IN} (W) and the Resulting removal efficiency in %.

Experiment (#)	CH ₄ (ppm)	Cl ₂ (ppm)	Residence time (s)	Power (W)	Removal efficiency (%)
Exp.E					
1	3.3805 ± 6E-03	30 ± 3	62.7 ± 1.6	13.39 ± 0.03	22 ± 12
2	3.3984 ± 2E-03	20 ± 2	61.6 ± 1.7	13.36 ± 0.03	19.8 ± 1.9
3	3.3947 ± 3E-03	20 ± 2	61.4 ± 1.5	9.89 ± 0.03	16.7 ± 1.2
4	3.4014 ± 9E-04	20 ± 2	61.4 ± 1.5	17.50 ± 0.03	23.1 ± 1.9
5	3.3282 ± 5E-03	40 ± 4	61.0 ± 1.5	13.43 ± 0.03	35 ± 3
6	3.3309 ± 5E-03	40 ± 4	61.1 ± 1.6	9.92 ± 0.03	29.3 ± 1.6
7	3.3312 ± 4E-03	40 ± 4	61.0 ± 1.6	17.47 ± 0.03	39 ± 6
8	3.4096 ± 6E-03	50 ± 5	60.7 ± 1.5	13.43 ± 0.03	40 ± 5
9	3.4444 ± 3E-03	50 ± 5	60.6 ± 1.5	9.90 ± 0.03	35 ± 2
10	3.4377 ± 3E-03	50 ± 5	60.6 ± 1.5	17.49 ± 0.03	45 ± 4
11	3.3575 ± 5E-03	60 ± 6	60.4 ± 1.5	13.43 ± 0.03	47 ± 2
12	3.3800 ± 7E-03	60 ± 6	60.4 ± 1.5	9.90 ± 0.03	41.0 ± 1.9
13	3.3604 ± 3E-03	60 ± 6	60.3 ± 1.6	17.49 ± 0.03	54 ± 2
14	3.4122 ± 3E-03	70 ± 7	60.1 ± 1.6	13.43 ± 0.03	53 ± 3
15	3.4414 ± 1.5E-03	70 ± 7	60.0 ± 1.6	9.90 ± 0.03	45 ± 3
16	3.4566 ± 8E-03	70 ± 7	59.8 ± 1.6	17.49 ± 0.03	59 ± 2
Exp.F					
1	3.5176 ± 6E-03	50 ± 5	162 ± 3.4	6.75 ± 0.02	28.0 ± 0.3
2	3.5475 ± 1.1E-03	50 ± 5	162 ± 3.4	9.74 ± 0.02	37.3 ± 0.3
3	3.5668 ± 1.8E-03	50 ± 5	161 ± 3.4	12.17 ± 0.03	46.83 ± 0.1
4	3.5920 ± 1.0E-03	50 ± 5	161 ± 3.4	14.63 ± 0.03	53.77 ± 0.1
5	3.6162 ± 1.9E-03	50 ± 5	161 ± 3.3	17.18 ± 0.03	55.2 ± 0.2
6	3.6425 ± 3E-03	50 ± 5	160 ± 3.4	19.73 ± 0.03	58.0 ± 0.3
7	3.6592 ± 1.2E-03	50 ± 5	160 ± 3.4	22.32 ± 0.03	59.2 ± 0.3

D1 CH₄ experimental results

In Tables D1 - D3 the four varying parameters; [CH₄]_{Initial}, [Cl₂], t_R and P_{IN} are presented for each experiment alongside
510 the resulting RE% . Table 4 summarizes the experiments done in the study.

Table D3. Data from exp. G - I. Columns: Experimental steps, [CH₄] in ppm, [Cl₂] in ppm, Residence time in seconds, Power in watts and the Resulting removal efficiency in %. **: The [CH₄] values are calculated based on trend fitting

Experiment (#)	CH ₄ (ppm)	Cl ₂ (ppm)	Residence time (s)	Power (W)	Removal efficiency (%)
Exp.G					
1	3.5594 ± 1.7E-03	50 ± 5	167 ± 3.5	14.46 ± 0.03	47.4 ± 1.2
2	3.2339 ± 1.3E-03	50 ± 5	168 ± 3.5	14.49 ± 0.03	54.7 ± 0.5
3	2.9339 ± 9E-04	50 ± 5	168 ± 3.5	14.56 ± 0.03	60.8 ± 0.5
4	2.684 ± 4E-02	50 ± 5	167 ± 3.6	14.60 ± 0.03	66.2 ± 0.6
5	2.2942 ± 3E-03	50 ± 5	164 ± 3.4	14.63 ± 0.03	69.6 ± 0.3
6	1.9817 ± 6E-04	50 ± 5	164 ± 3.5	14.46 ± 0.03	72.0 ± 0.4
7	1.6982 ± 7E-04	50 ± 5	166 ± 3.4	14.46 ± 0.03	74.1 ± 0.6
8	1.3899 ± 3E-04	50 ± 5	163 ± 3.5	14.46 ± 0.03	77.2 ± 0.7
9	3.8333 ± 7E-03	50 ± 5	162 ± 3.4	14.70 ± 0.03	60.3 ± 0.4
10	4.1285 ± 1.9E-03	50 ± 5	161 ± 3.4	14.63 ± 0.03	60.2 ± 0.2
11	3.5053 ± 1.7E-03	50 ± 5	161 ± 3.4	14.63 ± 0.03	64.0 ± 0.2
12	3.2045 ± 9E-04	50 ± 5	161 ± 3.4	14.63 ± 0.03	66.1 ± 0.3
Exp.H					
1	1.9857 ± 8E-04	50 ± 5	164 ± 3.4	14.77 ± 0.03	68 ± 3
2	1.9872 ± 1.0E-03	50 ± 5	261 ± 5.9	14.77 ± 0.03	88.1 ± 1.3
3	1.9955 ± 1.0E-03	50 ± 5	348 ± 8.3	14.77 ± 0.03	92 ± 5
4	1.9995 ± 8E-04	50 ± 5	357 ± 8.9	17.36 ± 0.03	94 ± 5
5	2.0099 ± 8E-04	50 ± 5	342 ± 8.3	19.94 ± 0.03	96 ± 4
6**	2.0021 ± 2E-03	50 ± 5	342 ± 8.2	22.80 ± 0.03	98.99 ± 0.1
7**	2.0046 ± 3E-03	50 ± 5	265 ± 25	22.80 ± 0.03	96.7 ± 0.3
8**	2.0061 ± 4E-03	50 ± 5	173 ± 20	22.80 ± 0.03	87.33 ± 0.1
9**	2.0076 ± 6E-03	50 ± 5	128 ± 10	22.80 ± 0.03	77.30 ± 0.1
Exp.I					
1	2.0471 ± 7E-04	50 ± 5	164 ± 3.4	7.92 ± 0.03	46.1 ± 1.8
2	2.0565 ± 9E-04	50 ± 5	164 ± 3.5	10.13 ± 0.03	56.6 ± 0.2
3	2.0586 ± 1.0E-03	50 ± 5	163 ± 3.5	12.54 ± 0.03	64.29 ± 0.1
4	2.0606 ± 1.1E-03	50 ± 5	163 ± 3.6	15.14 ± 0.03	70.31 ± 0.1
5	2.0627 ± 1.1E-03	50 ± 5	164 ± 3.6	17.71 ± 0.03	75.09 ± 0.1
6	2.0690 ± 1.4E-03	50 ± 5	162 ± 3.6	20.63 ± 0.03	80.28 ± 0.07
7	2.0710 ± 1.5E-03	50 ± 5	161 ± 3.5	23.63 ± 0.03	83.25 ± 0.04

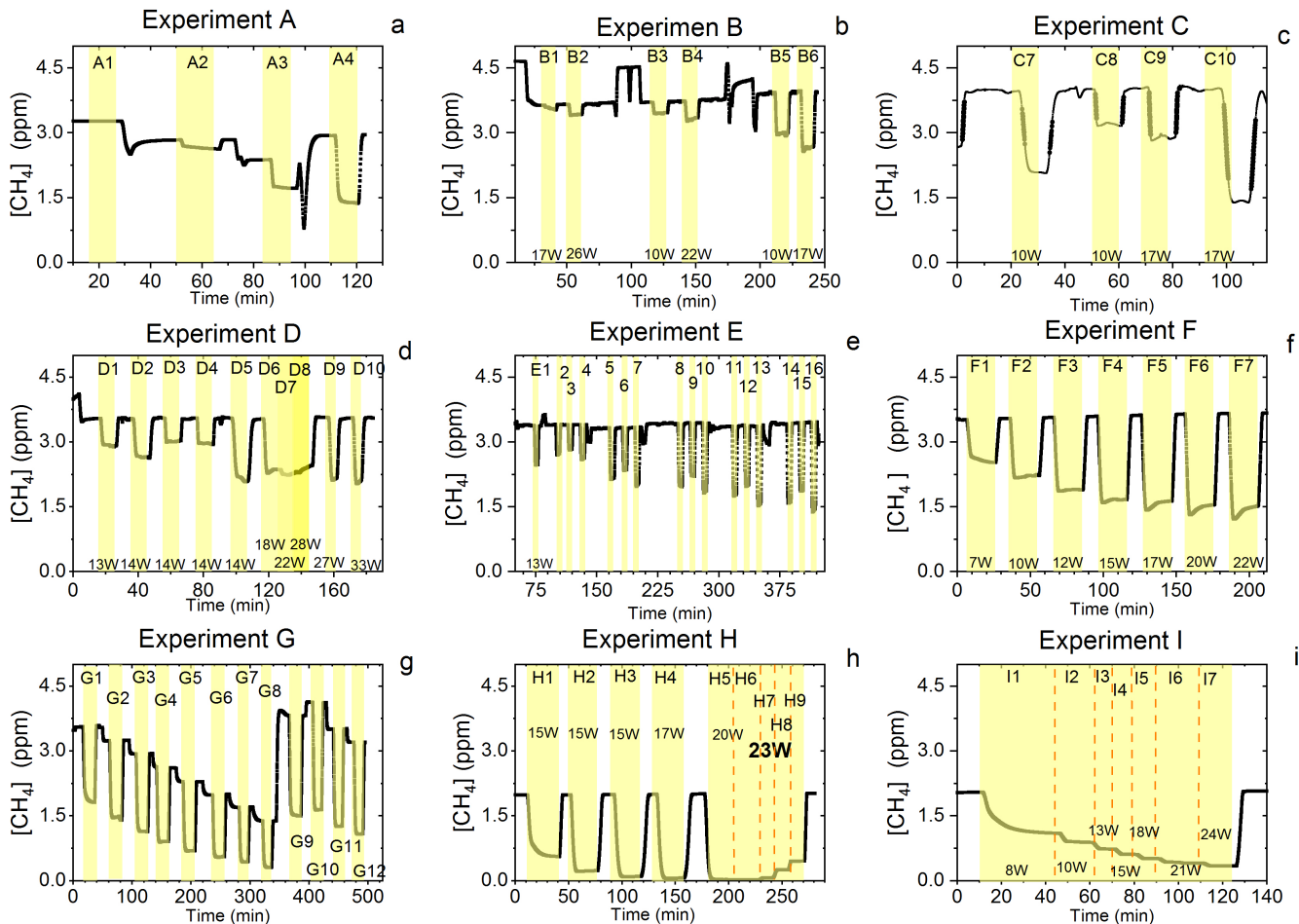


Figure D1. Exp. A-I is shown. Each illuminated step has been highlighted. **a.** The CH_4 is seen as a function of time. The $[\text{Cl}_2]$ is varied. **b.** The light intensity and $[\text{Cl}_2]$ are varied. **c.** Steps 7-10 highlighted. The light intensity and t_R are varied. **d.** Steps 1-10 are highlighted. The light intensity and t_R are varied. **e.** Steps 1-16 are highlighted. The light intensity and $[\text{Cl}_2]$ are varied. Following the initial illumination at 13 W the sample was illuminated at three different p_{IN} for five different chlorine concentrations. The p_{IN} was in the order 13W, 10W and 17W with chlorine steps 20, 40, 50, 60 and 70 ppm. **f.** Steps 1-7 are highlighted. The light intensity are varied. **g.** Steps 1-12 are highlighted. The CH_4 level is varied, while the light intensity is kept the same. **h.** Steps 1-9 are highlighted. The light intensity and t_R are varied. **i.** Steps 1-7 are highlighted. The light intensity are varied. Prolonged and stable photolysis enabled due to cooling. Increasing levels of p_{IN} for the photochemical chamber defines the seven different steps.

D1.1 Setup 1 (HPXL) experiments

The xenon-lamp experiments shown in Figure D1a were performed to confirm that the Cl_2 added to the gas-mix could make it to the photolysis-chamber. The RE% of methane was found as a result of varying the $[\text{Cl}_2]$ to 16.7, 25, 50, and 92 ppm as seen in Figure D2g. Each concentration step was given 10 minutes to stabilize before the xenon-lamp was turned on for ten minutes.

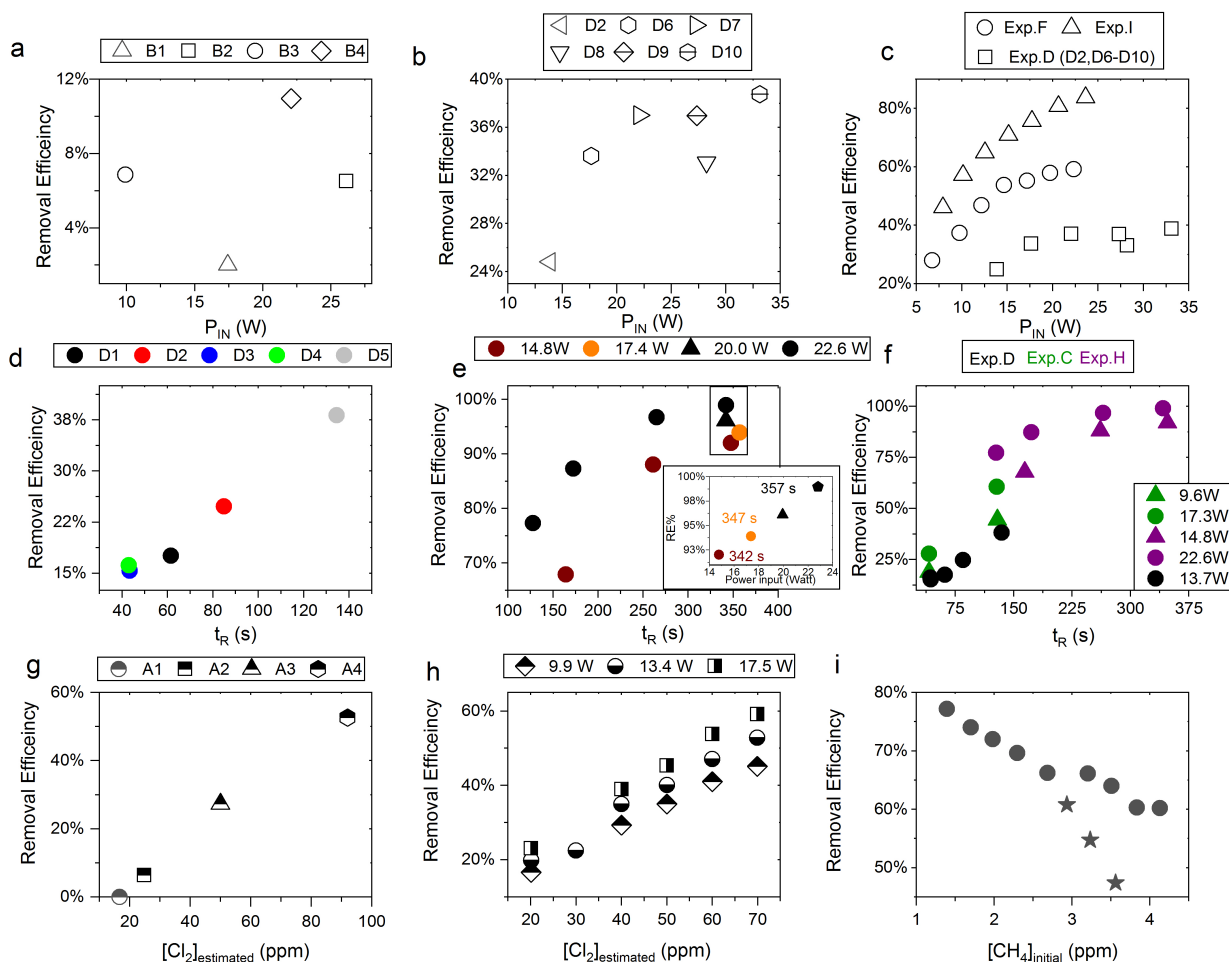


Figure D2. **a.** RE% as a function of p_{IN} for exp. B1-B4. **b.** Experiment steps D2 and D6-D10: RE% as a function of p_{IN} (W). **c.** RE% of methane plotted against p_{IN} in W. The result from three experiments, D (Square), F (Circle) and I (Arrow) have different settings in t_R , $[CH_4]$ and $[Cl_2]$. **d.** Experimental steps D1-D5: t_R (s) in the photochemical device as a function of t_R in seconds. **e.** The resulting removal efficiencies of exp. H plotted against t_R . An additional zoom inset Figure on the four points around 350 s reveals the removal effect plotted against power. **f.** RE% of methane plotted against t_R in s. The result from three experiments, D (Black), C (Green) and H (Purple) have different settings in p_{IN} , $[CH_4]$ and $[Cl_2]$. **g.** RE% as a function of $[Cl_2]$ in ppm for Xenon lamp exp. A. **h.** Resulting RE% plotted against $[Cl_2]$ in ppm for exp. steps E2-E16. Three different power settings are used. 9.9 W (Diamond), 13.4 W (Circle) and 17.5 W (Square). **i.** The RE% is displayed as a function of the initial methane concentration with the remaining fixed parameters such as Cl_2 mixing ratio, t_R , and p_{IN} . The three points (Star) in the Figure represent steps suffering from early- experiments-deviation.

515 The gas provided to the system was a dynamic mix of flows from three different flasks (see table Gas flasks Table B1). Due to this, it was possible to vary the abundance of chlorine while keeping $[CH_4]$ constant. The experiment confirmed that the level

Table D4. Table summarizing experiments and setups. FC:Flow-controlled, PC: Pressure-controlled, CWL: Chlorine waste line

Setup	Description	Experiment
1	High-Pressure Xenon lamp with FC CWL	A
2	Single tube hexagonal photochemical device with FC CWL	B
3	Single tube hexagonal photochemical device with PC CWL	C, D, E
4	Multiple tubes hexagonal photochemical device with PC CWL	F, G, H, I
5	Multiple tubes hexagonal photochemical device with PC CWL (N ₂ O)	J , K
6	Multiple tubes hexagonal photochemical device with PC CWL and sofnocat (N ₂ O)	L

of Cl₂ could be controlled and that higher levels resulted in greater depletion of methane.

D1.2 Setup 2 (Single tube, flow controlled chlorine waste line) experiments

520 In exp. B, P_{IN} was varied in steps one to four, presented in Figure D1b. The aim was to determine the effect of varying light intensity. Figure D2a shows the RE% as a function of p_{IN} for experiments one to four. The initial methane concentration is maintained at 3.68 ± 0.02 ppm. Step one and two are both examples of the start-up-deviation. At the time of step three and four, sufficient flushing had taken place. e. The chlorine concentration was increased from 16.7 to 50 ppm starting with step

Table D5. exp. B. The three experimental steps clearly shows an increasing RE% as the p_{IN} and the Cl₂ mixing ratio are increased

Step (#)	CH ₄ (ppm)	Cl ₂ (ppm)	Residence time (s)	Power (W)	RE% (%)
B3	$3.7069 \pm 1.1 \cdot 10^{-4}$	16.7 ± 1.5	62.2 ± 1.5	9.91 ± 0.03	6.87 ± 0.01
B5	$3.919 \pm 1.4 \cdot 10^{-3}$	50 ± 5	61.0 ± 1.4	9.92 ± 0.03	23.91 ± 0.05
B6	$3.945 \pm 1.3 \cdot 10^{-3}$	50 ± 5	61.4 ± 1.4	16.59 ± 0.03	32.69 ± 0.04

5. The four relevant variables and resulting RE% can be seen in Table D5. [Cl₂] was increased by a factor of 2.5 between
525 steps 3 and 5. The increase results in a 3.5 fold increase of RE%. Furthermore, the p_{IN} is increased when going from step 5 to 6 which also leads to an increase in RE%. The comparison between these three steps, the positive relation for both chlorine concentration and p_{IN} on the RE% was confirmed.

D1.3 Setup 3 (Single tube, pressure controlled chlorine waste line) experiments

530 Four experiments (C, D and E) used this setup. Exp. C presented in Figure D1c was carried out with constant supply of [Cl₂] at 50 ppm and [CH₄] at 3.981 ± 0.018 ppm. Step two and three had the same t_R , as does step one and four. In addition, the experiments vary in p_{IN} as can be seen in Table D6. Table D6 shows how the combination of increased t_R and p_{IN} yields a

higher RE%. The exp. D was carried out with $[Cl_2]$ kept constant at 32 ppm. The initial methane concentration was maintained

Table D6. Exp. C

Experiment (#)	CH ₄ (ppm)	Cl ₂ (ppm)	Residence time (s)	Power (W)	RE% (%)
C1	$3.957 \pm 5 \cdot 10^{-3}$	50 ± 5	41.4 ± 1.0	9.63 ± 0.03	18.90 ± 0.11
C2	$4.0301 \pm 5 \cdot 10^{-4}$	50 ± 5	41.4 ± 1.0	17.30 ± 0.03	27.83 ± 0.06
C3	$3.955 \pm 2 \cdot 10^{-3}$	50 ± 5	129 ± 3	9.63 ± 0.03	44.51 ± 0.3
C4	$3.986 \pm 9 \cdot 10^{-4}$	50 ± 5	128 ± 3	17.30 ± 0.03	60.6 ± 0.5

at 3.547 ± 0.005 ppm. Similarly to exp. C the t_R and p_{IN} were varied. Steps one to five are carried out with the same p_{IN}
535 in the device but with varying residence times, see Figure D2f and D2d. In Figure D2f the data for exp. D exhibits a clear
agreement between t_R and RE% . The longer t_R within the photochamber results in greater removal efficiencies. Steps two
and six to ten are carried out with the same t_R but with varying p_{IN} , see Figure D2c and D2b.
The experimental steps of exp. E, Figure D1e, were held the same initial methane concentration at 3.39 ± 0.01 ppm and
the same t_R at 60.82 ± 0.18 s. Throughout the experiments, three levels of p_{IN} were tested against varied levels of Cl_2 mix-
540 ing ratio spanning in the range 20 - 70 ppm. Figure D2h presents, looking at 20 ppm Cl_2 , that a greater p_{IN} yields higher RE%.

D1.4 Setup 4 (Multiple tubes, pressure controlled chlorine waste line) experiments

Four experiments (F, G, H and I) were done with this setup. The exp. F, Figure D1f, was run at a constant level of $[CH_4]_{initial}$
at 3.593 ± 0.019 ppm and $[Cl_2]$ at 50 ± 5 ppm. At a flow kept at 15.5 ml min^{-1} the t_R in the photochamber was maintained
545 at 161.06 ± 3 s. Across exp. F the step-wise changes were made for p_{IN} ranging from 6.75-22.92 W. The daily measurement
is presented in Figure D1f; where the removal for the steps, with the exception of the first step, is characterized by an initial
RE% but this efficiency drops during the first five minutes of illumination. The relationship found between removal and p_{IN}
for exp. F can be seen in Figure D2c.

Exp. G was carried out with a step-wise change of $[CH_4]_{initial}$ in the range 1.39 to 4.13 ppm, at constant t_R of 164 s, $[Cl_2]$
550 at 50 ppm, and p_{IN} 14.6 W. The daily result can be seen in Figure D1g, where the improvement of silicone removal can
be observed from stable levels of RE%. As can be seen in Figure D2i decreasing the initial methane concentration yields, as
expected, a greater RE% .

Exp.H was carried out with the constant $[CH_4]_{initial}$ at 2.000 ± 0.003 ppm and Cl_2 mixing ratio at 50 ± 5 ppm, but with
mixed settings of t_R and power. Step H1-H3 were done with constant power at 14.8 W with t_R increasing from 164-350 s.
555 Then keeping t_R around 350 s three steps of increasing power were tested, ranging from 14.8-22.8 W. In between step H4 and
H5 a fan was installed. The final three step were kept at 22.8 W and stepped through reduced t_R from 342-130 s.

Exp. I was carried out with $[CH_4]_{initial}$ maintained around 2.01 ± 0.01 ppm, $[Cl_2]$ at 50 ppm and the t_R held at 163.1 ± 0.4
s. The only parameter varied was the p_{IN} to the photochemical device. The light was turned at 7.9 W and was left on for the

duration of the experiments with a step-wise increase in P_{IN} after stable removal had been maintained for 5 min. The resulting methane concentration can be seen in Figure D1i. $[CH_4]$ increases throughout the experiments due to the chlorine-pressure-decline. For the purpose of calculating RE% , the expected $[CH_4]$ for each of the steps was fitted from the initial $[CH_4]$ and the end $[CH_4]$; $CH_4 = 0.0002 \cdot t + 2.0461$. The relative median values of initial methane and t_R were chosen in order to best resolve the effects of varying p_{IN} . As the removal effect approaches 100 % asymptotically, the sensitivity to changes will be greater at lower removal values.

The results presented for exp. I in Figure D2c can be compared to the results from exp. D and F and represents the improvements implemented to the system. Unlike for those experiments, the trend of exp. I is explained by one trend asymptotically approaching 100 % removal.

D1.5 Comparison

. Figure D2c shows a comparison of three different experiments where p_{IN} was varied. When comparing experiments F and I the improvement in performance of the device is clear. However, even if t_R and $[Cl_2]$ are identical, the initial methane concentration of exp. F is 3.59 ppm compared to exp. I at 2.096 ppm. Exp. D alone shares some P_{IN} levels and is operated at the same initial methane level as exp. F. The t_R and $[Cl_2]$ are lower and a lesser removal is accordingly expected. Hence, the main thing to observe is behavior at higher P_{IN} . The efficiency of the photochamber decreases as seen in exp. D and F. The improvements done on the photochamber and installation of a fan to cold the photochemical chamber have prolonged the lifetime of the chamber and improved efficiency.

Figure D2f shows a comparison of three different experiments where t_R was varied and in some cases P_{IN} as well. t_R is improved in the manner that the MTH-PD setup made it possible to obtain higher t_R and more efficient use of the photochemical chamber. The experiments with a single tube do not have long residence times. As seen in Figure D2f longer t_R greatly improves the RE% and is, therefore, essential to further improve the setup.

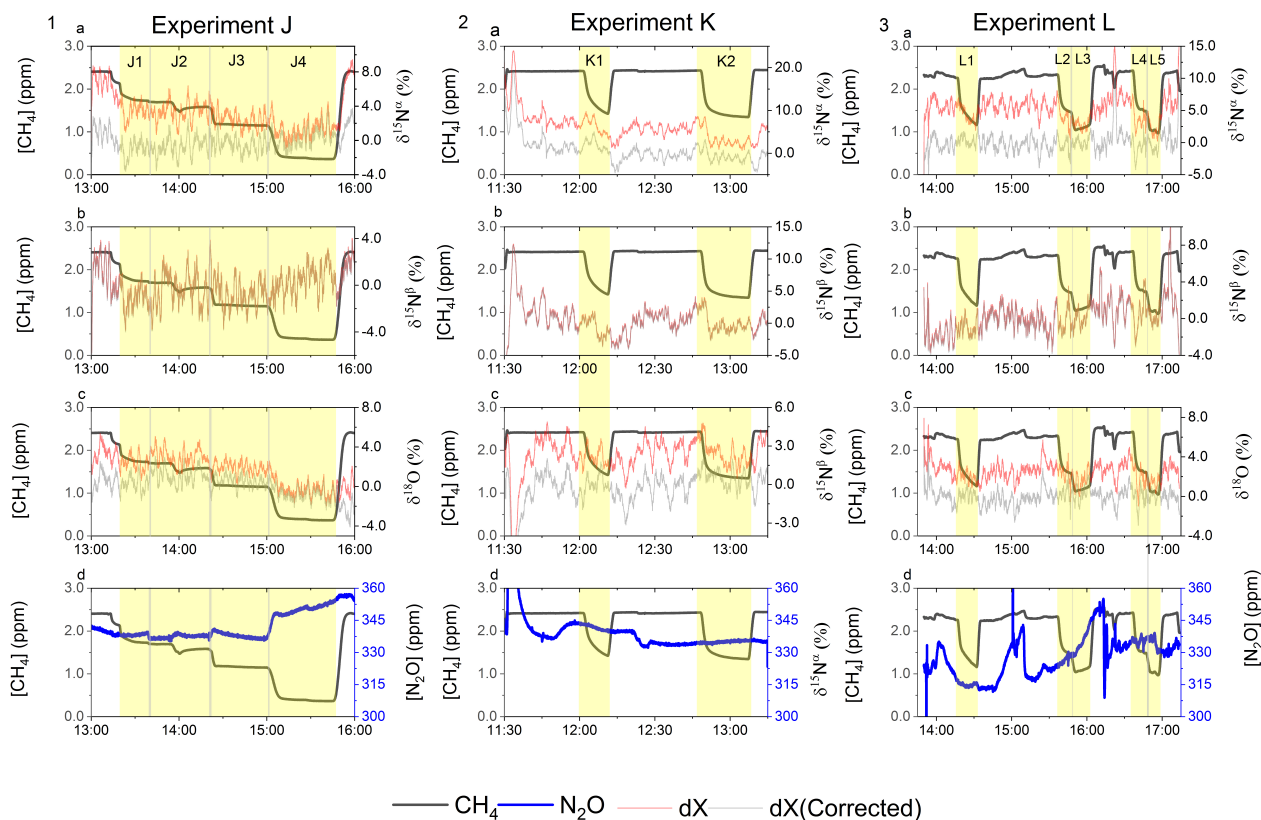


Figure D3. Results from the three experiments J, K and L using the G5131-i for N₂O isotope measurements. CH₄ level is depicted in each figure in ppm along the first y-axis. Highlights indicate the several different oxidation settings. **Row 1** Measurements of $\delta^{15}\text{N}^{\alpha}$ in ‰ plotted along the second y-axis. Red highlights a 100 s averaged measured values corrected for O₂, CO and CO₂ effects, while grey indicates a 100 s average value that have been corrected for all interference including CH₄. **Row 2** Measurements of $\delta^{15}\text{N}^{\beta}$ in ‰ plotted along the second y-axis. Red highlights a 100 s averaged measured values corrected for O₂, CO and CO₂ effects, while grey indicates a 100 s average value that have been corrected for all interference including CH₄. **Row 3** Measurements of $\delta^{18}\text{O}$ in ‰ plotted along the second y-axis. Red highlights a 100 s averaged measured values corrected for O₂, CO and CO₂ effects, while grey indicates a 100 s average value that have been corrected for all trace-gas interference including CH₄. **Row 4** Measurements of [N₂O] in ppb shown in blue. Variation observed correspond to fluctuations in the mixing of the three gasses. **Exp. J** In this experiment the light was turned on throughout the entire experiment, with the experimental steps corresponding to changes in t_R . **Exp. K** In this experiment two experimental steps were used with different power settings. **Exp. L** In this experiment the a softocat trap was used in the first three experimental steps, while 4 and 5 were completed without. The variation between experimental steps correspond to changes in t_R .

From the experiment investigating the compatibility of the removal method and the analysis of N₂O, it was found that the oxidization had no effect on the N₂O abundance nor isotopic composition. It was however discovered that the oxidation path for CH₄ terminated at CO, as the isotopic signal changed matching the interference of CO. To remove this effect a softnocat trap was implemented, which oxidize the CO to CO₂. By applying the tracegas and matrix corrections described in Harris et al. (2020), it was found that the isotopic levels remained stable across the oxidation. Variation observed in the N₂O was due to the unstable supply of Cl₂, resulting in slight shifts in the dilution. The value of $\delta^{15}\text{N}^\alpha$ and $\delta^{18}\text{O}$ were both found to approach the unaffected target value during the oxidation as was hoped. Results are shown in Figure D3

Appendix E: Kintecus reactions and results

The results from the kinetic model are shown in Figure E1.

Table E1. JPL: Burkholder et al. (2020).* Third order rate expression in the units ($\text{cm}^6 \text{ molecules}^{-2} \text{ s}^{-1}$). Hossaini: Hossaini et al. (2016)

Reaction	Reaction Rate Coefficient ($\text{cm}^3 \text{ molecules}^{-1} \text{ s}^{-1}$)	Reference
$\text{Cl}_2 \rightarrow 2 \text{ Cl}$	X	
$\text{Cl} + \text{Cl} + \text{M} \rightarrow \text{Cl}_2 + \text{M}$	1.29E-32*	Baulch et al. (1981)
$\text{O}_2 + \text{CH}_3 \rightarrow \text{CH}_3\text{O}_2$	1.79E-12	Atkinson et al. (1989)
$\text{O}_2 + \text{CH}_3\text{O} \rightarrow \text{CH}_2\text{O} + \text{HO}_2$	1.65E-15	Orlando et al. (2003)
$\text{O}_2 + \text{HCO} \rightarrow \text{CO} + \text{HO}_2$	5.20E-12	Atkinson et al. (2001)
$\text{O}_2 + \text{CH}_2\text{Cl} \rightarrow \text{CH}_2\text{ClO}_2$	2.91E-12	JPL
$\text{Cl} + \text{CH}_3\text{O} \rightarrow \text{CH}_2\text{O} + \text{HCl}$	1.91E-11	Daële et al. (1996)
$\text{Cl} + \text{CH}_3\text{OH} \rightarrow \text{CH}_3\text{O} + \text{HCl}$	5.50E-11	JPL
$\text{Cl} + \text{CH}_2\text{O} \rightarrow \text{HCO} + \text{HCl}$	7.32E-11	JPL
$\text{Cl} + \text{Cl}_2\text{O} \rightarrow \text{Cl}_2 + \text{ClO}$	9.60E-11	JPL
$\text{Cl} + \text{CH}_3\text{Cl} \rightarrow \text{CH}_2\text{Cl} + \text{HCl}$	4.98E-13	JPL
$\text{Cl} + \text{CH}_2\text{Cl}_2 \rightarrow \text{CHCl}_2 + \text{HCl}$	3.57E-13	JPL
$\text{Cl} + \text{CCl}_3 \rightarrow \text{CCl}_4$	6.51E-11	Ellermann (1992)
$\text{Cl} + \text{CHCl}_3 \rightarrow \text{HCl} + \text{CCl}_3$	1.20E-13	JPL
$\text{Cl} + \text{CH}_3\text{O}_2 \rightarrow \text{CH}_3\text{O} + \text{ClO}$	1.60E-10	JPL
$\text{Cl} + \text{CH}_3\text{O}_2 \rightarrow \text{CH}_2\text{O}_2 + \text{HCl}$	1.60E-10	JPL
$\text{Cl} + \text{CH}_4 \rightarrow \text{CH}_3 + \text{HCl}$	1.07E-13	Bryukov et al. (2002)
$\text{Cl} + \text{CHClO} \rightarrow \text{HCl} + \text{Cl} + \text{CO}$	7.79E-13	Atkinson et al. (2001)
$\text{Cl} + \text{H}_2\text{O}_2 \rightarrow \text{HCl} + \text{HO}_2$	4.10E-13	JPL
$\text{Cl} + \text{CH}_3 \rightarrow \text{CH}_3\text{Cl}$	1.61E-12	Kaiser (1993)
$\text{Cl}_2 + \text{CH}_2\text{Cl} \rightarrow \text{CH}_2\text{Cl}_2 + \text{Cl}$	2.54E-13	Seetula (1998)
$\text{Cl}_2 + \text{CHCl}_2 \rightarrow \text{CHCl}_3 + \text{Cl}$	2.25E-14	Seetula (1998)
$\text{Cl}_2 + \text{CH}_3 \rightarrow \text{CH}_3\text{Cl} + \text{Cl}$	1.55E-12	Eskola et al. (2008)
$\text{Cl}_2 + \text{HCO} \rightarrow \text{CHClO} + \text{Cl}$	5.59E-12	Timonen et al. (1988)
$\text{Cl}_2 + \text{OH} \rightarrow \text{HClO} + \text{Cl}$	6.42E-14	Atkinson et al. (2007)

Table E2. JPL: Burkholder et al. (2020).* Third order rate expression in the units ($\text{cm}^6 \text{ molecules}^{-2} \text{ s}^{-1}$). Hossaini: Hossaini et al. (2016)

Reaction	Reaction Rate Coefficient ($\text{cm}^3 \text{ molecules}^{-1} \text{ s}^{-1}$)	Reference
$\text{OH} + \text{CH}_4 \rightarrow \text{CH}_3 + \text{H}_2\text{O}$	6.30E-15	Bonard et al. (2002)
$\text{OH} + \text{CH}_3\text{OOH} \rightarrow \text{H}_2\text{O} + \text{CH}_3\text{O}_2$	7.40E-12	JPL
$\text{OH} + \text{CH}_3\text{OOH} \rightarrow \text{CH}_2\text{O} + \text{OH} + \text{H}_2\text{O}$	7.40E-12	JPL
$\text{OH} + \text{CH}_2\text{O} \rightarrow \text{HCO} + \text{H}_2\text{O}$	8.50E-12	JPL
$\text{OH} + \text{HCl} \rightarrow \text{Cl} + \text{H}_2\text{O}$	7.80E-13	JPL
$\text{OH} + \text{HClO} \rightarrow \text{ClO} + \text{H}_2\text{O}$	5.00E-13	Atkinson et al. (2007)
$\text{OH} + \text{CH}_2\text{Cl}_2 \rightarrow \text{CHCl}_2 + \text{H}_2\text{O}$	1.00E-13	JPL
$\text{OH} + \text{CHCl}_3 \rightarrow \text{CCl}_3 + \text{H}_2\text{O}$	1.00E-13	JPL
$\text{OH} + \text{CH}_3\text{O} \rightarrow \text{CH}_2\text{O} + \text{H}_2\text{O}$	3.01E-11	JPL
$\text{OH} + \text{CH}_3\text{OH} \rightarrow \text{CH}_3\text{O} + \text{H}_2\text{O}$	1.40E-13	Atkinson et al. (2001)
$\text{OH} + \text{CH}_3 \rightarrow \text{CH}_3\text{OH}$	9.30E-11	Oser et al. (1992)
$\text{OH} + \text{CH}_2\text{ClOOH} \rightarrow \text{CH}_2\text{ClO}_2 + \text{H}_2\text{O}$	3.60E-12	Hossaini
$\text{OH} + \text{CH}_2\text{ClOH} \rightarrow \text{CH}_3\text{O} + \text{HClO}$	4.54E-14	Hossaini
$\text{OH} + \text{H}_2\text{O}_2 \rightarrow \text{HO}_2 + \text{H}_2\text{O}$	1.80E-12	JPL
$\text{OH} + \text{CHClO} \rightarrow \text{Cl} + \text{CO} + \text{H}_2\text{O}$	3.20E-13	Hossaini
$\text{OH} + \text{ClO} \rightarrow \text{Cl} + \text{HO}_2$	1.80E-11	JPL
$\text{OH} + \text{ClO} \rightarrow \text{HCl} + \text{O}_2$	1.30E-12	JPL

Table E3. JPL: Burkholder et al. (2020).* Third order rate expression in the units ($\text{cm}^6 \text{ molecules}^{-2} \text{ s}^{-1}$).** First order rate expression in the units s^{-1} Hossaini: Hossaini et al. (2016)

Reaction	Reaction Rate Coefficient ($\text{cm}^3 \text{ molecules}^{-1} \text{ s}^{-1}$)	Reference
$\text{HO}_2 + \text{CH}_3\text{O}_2 \rightarrow \text{CH}_3\text{OOH} + \text{O}_2$	5.12E-12	JPL
$\text{HO}_2 + \text{Cl} \rightarrow \text{HCl} + \text{O}_2$	3.50E-11	JPL
$\text{HO}_2 + \text{Cl} \rightarrow \text{ClO} + \text{OH}$	9.30E-12	JPL
$\text{HO}_2 + \text{ClO} \rightarrow \text{HClO} + \text{O}_2$	6.90E-12	JPL
$\text{HO}_2 + \text{CH}_3\text{O} \rightarrow \text{CH}_2\text{O} + \text{H}_2\text{O}_2$	5.00E-13	Tsang and Hampson (1986)
$\text{HO}_2 + \text{HO}_2 \rightarrow \text{H}_2\text{O}_2 + \text{O}_2$	1.60E-12	Atkinson et al. (2004)
$\text{HO}_2 + \text{CH}_2\text{ClO}_2 \rightarrow \text{CH}_2\text{ClOOH} + \text{O}_2$	5.01E-12	Hossaini
$\text{HO}_2 + \text{CH}_2\text{ClO}_2 \rightarrow \text{CHClO} + \text{H}_2\text{O} + \text{O}_2$	5.01E-12	Hossaini
$\text{ClO} + \text{ClO} \rightarrow \text{O}_2 + \text{Cl}_2$	4.91E-15	JPL
$\text{ClO} + \text{ClO} \rightarrow 2\text{Cl} + \text{O}_2$	8.00E-15	JPL
$\text{ClO} + \text{Cl} + \text{M} \rightarrow \text{Cl}_2\text{O} + \text{M}$	1.56E-32*	Xu (2010)
$\text{ClO} + \text{CH}_3\text{O}_2 \rightarrow \text{Cl} + \text{O}_2 + \text{CH}_3\text{O}$	2.40E-12	JPL
$\text{ClO} + \text{CH}_3 \rightarrow \text{CH}_3\text{OCl}$	5.69E-11	Brudnik et al. (2009)
$\text{CH}_3\text{O}_2 + \text{CH}_3\text{O}_2 \rightarrow \text{CH}_3\text{O} + \text{CH}_3\text{O} + \text{O}_2$	3.50E-13	JPL
$\text{CH}_3\text{O}_2 + \text{CH}_3\text{O}_2 \rightarrow \text{CH}_3\text{OH} + \text{CH}_2\text{O} + \text{O}_2$	3.50E-13	JPL
$\text{CH}_3 + \text{CH}_3\text{O}_2 \rightarrow \text{CH}_3\text{O} + \text{CH}_3\text{O}$	4.50E-11	Pilling and Smith (1985)
$\text{CH}_3\text{O} + \text{CH}_3\text{O} \rightarrow \text{CH}_2\text{O} + \text{CH}_3\text{OH}$	3.85E-11	Hassinen and Koskikallio (1979)
$\text{CH}_2\text{ClO}_2 + \text{CH}_3\text{O}_2 \rightarrow \text{CH}_2\text{ClO} + \text{CH}_2\text{O} + \text{HO}_2$	2.50E-12	Hossaini
$\text{CH}_2\text{ClO}_2 + \text{CH}_3\text{O}_2 \rightarrow \text{CH}_2\text{ClOH} + \text{CH}_2\text{O} + \text{O}_2$	2.50E-12	Hossaini
$\text{CH}_2\text{ClO}_2 + \text{CH}_3\text{O}_2 \rightarrow \text{CHClO} + \text{CH}_3\text{OH} + \text{O}_2$	2.50E-12	Hossaini
$\text{CH}_2\text{ClO}_2 + \text{CH}_2\text{ClO}_2 \rightarrow \text{CH}_2\text{ClO} + \text{CH}_2\text{ClO} + \text{O}_2$	3.50E-12	Hossaini
$\text{CH}_2\text{Cl}_2 + \text{Cl} \rightarrow \text{CHCl}_2 + \text{HCl}$	3.57E-13	Atkinson et al. (2001)
$\text{CHCl}_2 + \text{Cl}_2 \rightarrow \text{CHCl}_3 + \text{Cl}$	2.25E-14	Seetula (1998)
$\text{CCl}_3 + \text{Cl} \rightarrow \text{CCl}_4$	6.51E-11	Ellermann (1992)
$\text{HCO} + \text{Cl}_2 \rightarrow \text{HC(O)Cl} + \text{Cl}$	5.59E-12	Timonen et al. (1988)
$\text{CH}_2\text{O}_2 \rightarrow \text{CO} + \text{H}_2\text{O}$	6.00E+04**	Maricq et al. (1994)

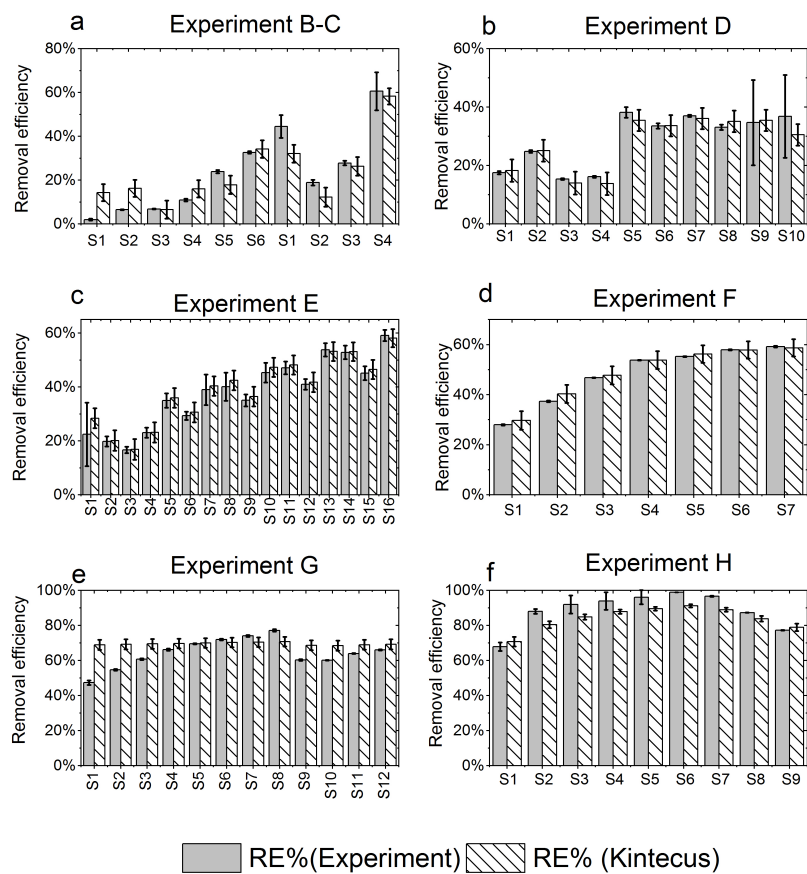


Figure E1. RE% as found experimentally (grey) and by model (white stripes). **a.** Exp.B and C **b.** Exp.D **c.** Exp.E **d.** Exp.F **e.** Exp.G **f.** Exp.H

590 *Author contributions.* Matthew S. Johnson, Merve Polat and Jesper Baldtzer Liisberg conceived and planned the experiments. Merve Polat and Jesper Baldtzer Liisberg carried out the experiments. Merve Polat, Jepser Baldtzer and Morten Krogsbøll planned and carried out the simulations. Merve Polat and Jesper Baldtzer Liisberg contributed to the interpretation of the results. Merve Polat and Jesper Baldtzer Liisberg wrote the manuscript in consultation with Thomas Blunier and Matthew S. Johnson. All authors provided critical feedback and helped shape the research, analysis and manuscript.

595 *Competing interests.* The authors declare that they have no conflict of interest.

Data availability. All data are available from the corresponding author upon request.

Acknowledgements. We thank the Copenhagen Center for Atmospheric Research (CCAR), the Centre for Ice and Climate and the University of Copenhagen. The authors thank Silvia Pugliese for her help with the reaction mechanism.

References

- Atkinson, R., Baulch, D., Cox, R., Hampson Jr, R. F., Kerr, J., and Troe, J.: Evaluated kinetic and photochemical data for atmospheric chemistry: supplement III. IUPAC subcommittee on gas kinetic data evaluation for atmospheric chemistry, Journal of Physical and Chemical Reference Data, 18, 881–1097, <https://doi.org/10.1063/1.555832>, 1989.
- Atkinson, R., Baulch, D., Cox, R., Crowley, J., Hampson Jr, R., Kerr, J., Rossi, M., and Troe, J.: Summary of evaluated kinetic and photochemical data for atmospheric chemistry, IUPAC Subcommittee on gas kinetic data evaluation for atmospheric chemistry, 20, 2001.
- Atkinson, R., Baulch, D., Cox, R., Crowley, J., Hampson, R., Hynes, R., Jenkin, M., Rossi, M., and Troe, J.: Evaluated kinetic and photochemical data for atmospheric chemistry: Volume I-gas phase reactions of Ox, HOx, NOx and SOx species, Atmospheric chemistry and physics, 4, 1461–1738, 2004.
- Atkinson, R., Baulch, D., Cox, R., Crowley, J., Hampson, R., Hynes, R., Jenkin, M., and Rossi, M.: Troe., J., Evaluated kinetic and photochemical data for atmospheric chemistry: Volume iii-gas phase reactions of inorganic halogens, Atmos Chem and Phys, 7, 981–1191, 2007.
- Baulch, D., Duxbury, J., Grant, S., and Montague, D.: Evaluated kinetic data for high temperature reactions. Volume 4. Homogeneous gas phase reactions of halogen-and cyanide-containing species, 1981.
- Bonard, A., Daële, V., Delfau, J.-L., and Vovelle, C.: Kinetics of OH radical reactions with methane in the temperature range 295- 660 K and with dimethyl ether and methyl-tert-butyl ether in the temperature range 295- 618 K, The Journal of Physical Chemistry A, 106, 4384–4389, <https://doi.org/10.1021/jp012425t>, 2002.
- Brudnik, K., Gola, A. A., and Jodkowski, J. T.: Theoretical kinetic study of the formation reactions of methanol and methyl hypohalites in the gas phase, Journal of molecular modeling, 15, 1061–1066, <https://doi.org/10.1007/s00894-009-0461-x>, 2009.
- Bryukov, M. G., Slagle, I. R., and Knyazev, V. D.: Kinetics of reactions of Cl atoms with methane and chlorinated methanes, The journal of physical chemistry A, 106, 10 532–10 542, <https://doi.org/10.1021/jp0257909>, 2002.
- Burkholder, J., Sander, S., Abbatt, J., Barker, J., Cappa, C., Crounse, J., Dibble, T., Huie, R., Kolb, C., Kurylo, M., et al.: Chemical kinetics and photochemical data for use in atmospheric studies; evaluation number 19, Tech. rep., Pasadena, CA: Jet Propulsion Laboratory, National Aeronautics and Space . . . , 2020.
- Cullis, C. and Willatt, B.: Oxidation of methane over supported precious metal catalysts, Journal of Catalysis, 83, 267–285, [https://doi.org/10.1016/0021-9517\(83\)90054-4](https://doi.org/10.1016/0021-9517(83)90054-4), 1983.
- Daële, V., Laverdet, G., and Poulet, G.: Kinetics of the reactions of CH₃O with Cl and ClO, International journal of chemical kinetics, 28, 589–598, [https://doi.org/10.1002/\(sici\)1097-4601\(1996\)28:8<589::aid-kin4>3.0.co;2-r](https://doi.org/10.1002/(sici)1097-4601(1996)28:8<589::aid-kin4>3.0.co;2-r), 1996.
- Ellermann, T.: Fine structure of the CCl₃ UV absorption spectrum and CCl₃ kinetics, Chemical physics letters, 189, 175–181, [https://doi.org/10.1016/0009-2614\(92\)85119-u](https://doi.org/10.1016/0009-2614(92)85119-u), 1992.
- Erlor, D. V., Duncan, T. M. and Murray, R., Maher, D. T., Santos, I. R., Gatland, J. R., Mangion, P., and Eyre, B. D.: Applying cavity ring-down spectroscopy for the measurement of dissolved nitrous oxide mole fractions and bulk nitrogen isotopic composition in aquatic systems: Correcting for interferences and field application., Limnology and Oceanography: Methods, 13, 391–401, <https://doi.org/10.1002/lom3.10032>, 2019.
- Eskola, A. J., Timonen, R. S., Marshall, P., Chesnokov, E. N., and Krasnoperov, L. N.: Rate constants and hydrogen isotope substitution effects in the CH₃ + HCl and CH₃ + Cl₂ reactions, The Journal of Physical Chemistry A, 112, 7391–7401, <https://doi.org/10.1021/jp801999w>, 2008.

- Harris, S. J., Liisberg, J., Xia, L., Wei, J., Zeyer, K., Yu, L., Barthel, M., Wolf, B., Kelly, B. F., Cendón, D. I., et al.: N₂O isotopocule measurements using laser spectroscopy: analyzer characterization and intercomparison, *Atmospheric Measurement Techniques*, 13, 2797–2831, <https://doi.org/10.5194/amt-13-2797-2020>, 2020.
- Hassinen, E. and Koskikallio, J.: Flash Photolysis of Methyl Acetate in Gas Phase. Products and Rate Constants of Reactions between Methyl, Methoxy and Acetyl Radicals, *Acta Chem. Scand., Ser. A*, 33, 625–630, <https://doi.org/10.3891/acta.chem.scand.33a-0625>, 1979.
- Hossaini, R., Chipperfield, M. P., Saiz-Lopez, A., Fernandez, R., Monks, S., Feng, W., Brauer, P., and Von Glasow, R.: A global model of tropospheric chlorine chemistry: Organic versus inorganic sources and impact on methane oxidation, *Journal of Geophysical Research: Atmospheres*, 121, 14–271, <https://doi.org/10.1002/2016jd025756>, 2016.
- Ianni, J.: Kintecus, Windows version, 3, 2012.
- Ibraim, E., Wolf, B., Harris, E., Gasche, R., Wei, J., Yu, L., Kiese, R., Eggleston, S., Butterbach-Bahl, K., Zeeman, M., et al.: Attribution of N₂O sources in a grassland soil with laser spectroscopy based isotopocule analysis, *Biogeosciences*, 16, 3247–3266, <https://doi.org/10.5194/bg-16-3247-2019>, 2019a.
- Ibraim, E., Wolf, N., Harris, E., Gasche, R., Wei, J., Yu, L., Kiese, R., Eggleston, S., Butterbach-Bahl, K., Zeeman, M., Tuzson, B., Emmenegger, L., Six, J., Henne, S., and Mohn, J.: Attribution of N₂O sources in a grassland soil with laser spectroscopy based isotopocule analysis, *Biogeosciences*, 16, 3247–3266, <https://doi.org/10.5194/bg-16-3247-2019>, 2019b.
- Ivanov, A. V., Trakhtenberg, S., Bertram, A. K., Gershenson, Y. M., and Molina, M. J.: OH, HO₂, and ozone gaseous diffusion coefficients, *The Journal of Physical Chemistry A*, 111, 1632–1637, <https://doi.org/10.1021/jp066558w>, 2007.
- Judeikis, H. S. and Wun, M.: Measurement of chlorine atom diffusion, *The Journal of Chemical Physics*, 68, 4123–4127, <https://doi.org/10.1063/1.436326>, 1978.
- Kaiser, E.: Pressure dependence of the rate constants for the reactions methyl+ oxygen and methyl+ nitric oxide from 3 to 104 torr, *The Journal of Physical Chemistry*, 97, 11 681–11 688, <https://doi.org/10.1021/j100147a022>, 1993.
- M. Zimnoch, J. Godlowska, J. M. N. and Rozanski, K.: Assessing surface fluxes of CO₂ and CH₄ in urban environment: a reconnaissance study in Krakow, Southern Poland, *Tellus*, 62B, 573–580, <https://doi.org/10.3402/tellusb.v62i5.16605>, 2010.
- Maricq, M. M., Szente, J. J., Kaiser, E., and Shi, J.: Reaction of chlorine atoms with methylperoxy and ethylperoxy radicals, *The Journal of Physical Chemistry*, 98, 2083–2089, <https://doi.org/10.1021/j100059a017>, 1994.
- Milchert, E., Goc, W., and Pelech, R.: Adsorption of CCl₄ from aqueous solution on activated carbons, *Adsorption Science & Technology*, 18, 823–837, <https://doi.org/10.1260/0263617001493846>, 2000.
- Moore, J. H., Davis, C. C., Coplan, M. A., and Greer, S. C.: Building scientific apparatus, Cambridge University Press, 2009.
- Nilsson, E. J. K., Eskebjerg, C., and Johnson, M. S.: A photochemical reactor for studies of atmospheric chemistry, *Atmospheric Environment*, 43, 3029–3033, <https://doi.org/10.1016/j.atmosenv.2009.02.034>, 2009.
- Orlando, J. J., Tyndall, G. S., and Wallington, T. J.: The atmospheric chemistry of alkoxy radicals, *Chemical reviews*, 103, 4657–4690, <https://doi.org/10.1002/chin.200412254>, 2003.
- Oser, H., Stothard, N., Humpfer, R., and Grotheer, H.: Direct measurement of the reaction methyl+ hydroxyl at ambient temperature in the pressure range 0.3–6.2 mbar, *The Journal of Physical Chemistry*, 96, 5359–5363, <https://doi.org/10.1021/j100192a034>, 1992.
- Pilling, M. J. and Smith, M. J.: A laser flash photolysis study of the reaction methyl+ molecular oxygen. fwdarw. methylperoxy (CH₃O₂) at 298 K, *The Journal of Physical Chemistry*, 89, 4713–4720, <https://doi.org/10.1021/j100268a014>, 1985.
- Pletcher, D. and Walsh, F. C.: Industrial electrochemistry, Springer Science & Business Media, 2012.

- Pugliese, S.: New Multiphase Photochemical Approach for Cl-initiated Methane and VOC Oxidation, Master's thesis, The University of Copenhagen, 2018.
- 675 Rigby, M., Montzka, S. A., Prinn, R. G., White, J. W., Young, D., O'Doherty, S., Lunt, M. F., Ganesan, A. L., Manning, A. J., Simmonds, P. G., et al.: Role of atmospheric oxidation in recent methane growth, *Proceedings of the National Academy of Sciences*, 114, 5373–5377, <https://doi.org/10.1073/pnas.1616426114>, 2017.
- Ryu, S. K. and Choi, S. R.: Activated carbon fibers for the removal of chemical warfare simulants, in: *Journal of the Ceramic Society of Japan, Supplement Journal of the Ceramic Society of Japan, Supplement 112-1, PacRim5 Special Issue*, pp. S1539–S1542, The Ceramic Society of Japan, 2004.
- 680 Seetula, J.: Kinetics of the $R + Cl_2$ ($R = CH_2Cl$, $CHBrCl$, CCl_3 and CH_3CCl_2) reactions. An ab initio study of the transition states, *Journal of the Chemical Society, Faraday Transactions*, 94, 3561–3567, 1998.
- Seinfeld, J. H. and Pandis, S. N.: *Atmospheric chemistry and physics: from air pollution to climate change*, John Wiley & Sons, 2016.
- Timonen, R. S., Ratajczak, E., and Gutman, D.: Kinetics of the reactions of the formyl radical with oxygen, nitrogen dioxide, chlorine, and bromine, *The Journal of Physical Chemistry*, 92, 651–655, <https://doi.org/10.1021/j100314a017>, 1988.
- 685 Tsang, W. and Hampson, R.: Chemical kinetic data base for combustion chemistry. Part I. Methane and related compounds, *Journal of physical and chemical reference data*, 15, 1087–1279, <https://doi.org/10.1063/1.555759>, 1986.
- Wolf, B., Merbold, L., Decock, C., Tuzson, B., Harris, E., Six, J., Emmenegger, L., and Mohn, J.: First on-line isotopic characterization of N_2O above intensively managed grassland, *Biogeosciences*, 12, 2517–2531, <https://doi.org/10.5194/bg-12-2517-2015>, 2015.
- 690 Xu, Z.F.; Lin, M.: Ab Initio Chemical Kinetic Study on Cl plus ClO and Related Reverse Processes, *J. Phys. Chem. A*, 114, 11 477–11 482, <https://doi.org/10.1021/jp102947w>, 2010.
- Yu, L., Harris, E., Lewicka-Szczebak, D., Barthel, M., Blomberg, M. R., Harris, S. J., Johnson, M. S., Lehmann, M. F., Liisberg, J., Müller, C., et al.: What can we learn from N_2O isotope data?—Analytics, processes and modelling, *Rapid Communications in Mass Spectrometry*, 34, e8858, 2020.